Using synthetic activity to design ultra-potent antibody cocktails

Hui Zhao[1]†, Michael Dodds[1]†, Michael Tasch[1], Mesfin Gewe[1], Anissa Martinez[1], Melanie Hutton[2], Kristie Keeney[1], Alex Pollock[1], Benjamin W. Jester[1], Nhi Khuong[1], Mia Zhang[1], Stacey Ertel[1], Colin Brady[1], Mark Heinnickel[1], Hannah Tabakh[1], Nathan Sanjaya[1], Kendra Cruickshank[1], Troy Paddock[1], Sarah Struyvenberg[1], Jason Dang[1], Tracy Saveria[1], Chelsea Shanitta[1], David Fletcher[1], Kristjan Sigmar[1], Lauren Goetsch[1], Caitlin Gamble[1], Steven J. Mileto[2], Ryan Heselpoth[3], Dena Lyras[2], Craig A. Behnke[1], Vincent Fischetti[3], Brian Finrow[1], and James M. Roberts[1,*]

[1]Lumen Bioscience, Seattle, WA

[2]Biomedicine Discovery Institute and Department of Microbiology, Monash University, Victoria, Australia

[3]Laboratory of Bacterial Pathogenesis and Immunity, Rockefeller University, New York, NY

†These two authors contributed equally

[*]Corresponding author. Email: jroberts@lumen.bio

Abstract: Drugs which independently inhibit a shared target or pathway can have synthetic activities that result in multiplicative instead of merely additive potencies. This characteristic of drug combinations can be quantified by expressing the potency of the combination as if it were a single agent. We show that by optimizing this quantity we can prospectively design drug cocktails with apparent potencies that far exceed any of its individual components. We illustrate the power of this approach, which is based on statistical design of experiments to select optimal drug combinations, and response surface methodology to determine optimal drug ratios, by building a drug cocktail comprised of three antibodies for treating *C. difficile* infection that is almost 1000-fold more potent than the current, clinically approved antibody monotherapy. High synthetic activities do not require unusual drug interactions, and therefore may be achievable much more readily than generally appreciated.

One-Sentence Summary: A development pathway is described for designing antibody cocktails with potencies that far exceed what is achievable with single antibodies

The remarkable efficacies of combination therapies like Harvoni (*1*), which revolutionized the treatment of hepatitis C, and the potent cocktail therapeutics for HIV (*2*) highlight how polypharmacology can address medical needs unmet by monopharmacology approaches. However, very few biologic drug cocktails have ever reached approval. New molecular and computational tools have removed one key barrier by accelerating the availability of large and diverse sets of candidate drugs and antibodies. Nevertheless, development of antibody cocktails has been largely limited to clinical evaluation of combinations of previously developed monotherapies or cocktail formulations to cover potential target diversity, rather than to directly improve potency. Moreover, dose selection is typically a simple 1:1 mixture, or in proportion to prior approved doses of the single agents. Given the range of performance characteristics it is unlikely that these defaults will be optimal. There is a critical emerging need for advanced methodologies that can identify not only optimal antibody combinations, but also predict antibody ratios for maximal combined efficacy.

Here we describe a new approach to discovering exceptionally potent antibody cocktails with levels of target neutralization that are likely unachievable with antibody monotherapies. A key feature of the approach is that it exploits the strikingly greater-than-additive potencies achieved by combinations of independently binding drugs, such as antibodies (*3*). The laws of orthosteric mass action are sufficient to explain these apparent synergies; they do not require unusual instances of allostery or cooperativity and therefore should be readily incorporated into strategies for developing new drug cocktails. We further show how response surface methodologies, which map multiple inputs (such as antibody concentrations, antibody potencies and target concentrations) onto a single output (such as cell viability), can be used to determine optimal antibody ratios in a cocktail. We illustrate this with a 3-antibody cocktail targeting *C. difficile*, a pathogen which causes severe, recurrent colitis and is associated with substantial morbidity and

mortality world-wide (*4*). This cocktail is greater than 1,000 times more potent than bezlotoxumab (*5*, *6*), the antibody monotherapy currently in clinical use.

C. difficile virulence is mediated by two homologous exotoxins, TcdA and TcdB (*7–10*). The toxins initially engage cell surface receptors on intestine epithelial cells, and after internalization enzymatically inhibit Rho family-GTPases. This disaggregates the cellular actin cytoskeleton thereby disrupting the integrity of the colonic epithelium (*11–13*), leading to severe colon pathology. The current balance of opinion is that human disease is primarily caused by TcdB (*6*, *9*, *14–18*).

Disruption of the actin cytoskeleton, and hence cell killing, by TcdB can be measured *in vitro* as a change in impedance using cells cultured on a surface embedded with microelectrodes (*19–21*). TcdB1 is the TcdB toxin type most frequently present in *C. difficile* isolates from infected patients (*22*). The concentration range of TcdB1 tested spanned the amounts reported in human patients with *C. difficile* infection (*23*). The following four-parameter sigmoid model was fit to data describing TcdB1 toxicity using nonlinear regression to minimize the sums of residuals squared:

$$Fraction\ Viable = 1 - \frac{T^H}{T^H + IC_{50}^H} \quad (1)$$

where Fraction Viability indicates the scaled [0-100%] results of the above assay; T is the concentration of TcdB1; IC_{50} is the concentration of TcdB1 eliciting half maximal reduction in viability; H is the steepness of the concentration-response relationship. At full TcdB activity, all the cells detach from the plate and the fractional viability is zero. The concentration of half-maximal reduction of cell viability by TcdB1 was IC_{50}=1.268 fM with a Hill slope coefficient of H=1.495 (Supplemental Table 1).

An inhibitor of T (for example an anti-TcdB antibody) reduces the free amount of T, such that the free fraction, f_T, is less than one. Equation 1 is modified to reflect activity only from the free fraction of, $f_T \cdot T$. Alternately, the effect of an inhibitor can be described as a fold-shift, α, in the potency of T, $IC_{50} \cdot \alpha$. While identical, the former formulation is more intuitive, but the latter form allows for a more compact mathematical representation and stable numerical estimation.

$$Fraction\ Viable = 1 - \frac{(f_T \cdot T)^H}{(f_T \cdot T)^H + (IC_{50})^H} = 1 - \frac{T^H}{T^H + (IC_{50} \cdot \alpha)^H} \quad \text{where } \alpha = {}^{1}/_{f_T} \qquad (2)$$

For antibody inhibition of a target:

$$f_T = \frac{T}{T + AT} = \frac{T}{T + \frac{T \cdot A}{K_A}} = \frac{1}{1 + \frac{A}{K_A}} \qquad (3)$$

Where A and AT are the concentration of the antibody and antibody-target complex, and K_A is an equilibrium constant that defines the concentration of A that halves the free fraction of T. Often, this dissociation equilibrium constant is referred to as "binding potency" or, simply, "potency". Table 1 ("Free Fraction of Target") expands Equation 3 for two or more binders, depending on the how the binders interact (see Supplemental Materials).

Conversion from f_T to α is the simple reciprocal, giving an alternative definition of K_A as the concentration that results in a two-fold increase in IC_{50}. Table 1 ("Fold-Shift of Target Potency") expands Equation 4 for two or more binders, depending on the how the binders interact (see Supplemental Materials).

$$\alpha = 1 + \frac{A}{K_A} \qquad (4)$$

If the concentration of an antibody target (e.g., toxin B) is in great excess of its potency ($T >> IC_{50}$), neutralization may require an antibody concentration that is not achievable *in vivo* or an antibody potency that is infeasibly high. In patients with untreated *C. difficile* infection, the concentration of TcdB is approximately 20 ng/ml (T=74.1 pM) (*23*). With this high toxin burden, $f_T=6.67\cdot10^{-6}$ is required to reduce the effective TcdB concentration to a level that would restore 80% of normal cell viability. This is equivalent to an α=150,000-fold shift in TcdB IC_{50}.

A single antibody with a K_A=30 pM would require A=5 μM to yield an α=150,000-fold shift in TcdB IC_{50} (Equation 4). Bezlotoxumab, a monoclonal antibody used to prevent recurrence of *C. difficile* infection, has a binding affinity in this range, but a 5 μM concentration is 4-fold higher than the transient peak serum level achieved by the current dosing regimen (*24*). Critically, due to the limitations of antibody partitioning into affected tissues, A=5 μM is approximately 100 to 1000-fold higher than the predicted concentration of bezlotoxumab at the site of infection in the intestinal lumen (*25*). This may explain why bezlotoxumab is only modestly effective at preventing *C. difficile* recurrence and must be administered concomitantly with antibiotics, which themselves reduce the TcdB burden 10 to 100-fold (*23*), presumably reducing TcdB concentration into a range where the fold shift in the TcdB IC_{50} is approachable.

Alternatively, a A=10 nM concentration of an antibody with a K_A=67 fM would be sufficient to neutralize this amount of TcdB to the same extent (Equation 4). Achieving this low K_A is extremely unlikely for any single antibody. In what follows, we show that it can be achieved by assembling a cocktail of three independently acting anti-TcdB single domain antibodies (VHHs), each of which on its own has a K_A similar to bezlotoxumab.

The synthetic activity of a drug cocktail depends critically upon whether the components act competitively or independently; for antibodies this would be exclusive versus simultaneous binding. The difference between these two cases rests, fundamentally, in the difference between taking the sum of effects (competitive) or the product of effects (independent), providing a geometric advantage to the independent case. These general solutions are illustrated in Table 1.

A panel of VHHs that bind to and neutralize TcdB has been previously described (*10*, *26–28*). Structural analyses showed that three of these – 5D, E3 and 7F – recognized distinct antigenic epitopes on TcdB (*28*). We used our spirulina platform (*29*) to express each of these VHHs, which were then purified as monomers or as 5HVZ-scaffolded dimers (*30*). Noncompetitive (independent) binding was confirmed by biolayer interferometry (fig. S1). Binding kinetics for the monomers and dimers were then measured using recombinant subdomains of TcdB that corresponded to the specific antigen-binding sites of each VHH (fig. S2). The apparent K_D for the homodimers were in the picomolar range. The dimeric versions of all three proteins displayed substantially greater avidity for TcdB than the corresponding monomeric versions, possibly due to the dimeric state of TcdB (*31*).

We evaluated inhibition of TcdB1 toxicity by each VHH homodimer (pp1005=5D, pp1006=E3, pp1007=7F), each binary mixture at 1:1 molar ratio, and the trinary mixture at 1:1:1 and 1:5:7 molar ratio of pp1005: pp1006: pp1007 (Fig. 1 and Table S1). As described more fully below, the 1:5:7 ratio was selected because it conveniently represents the relative amount of the VHHs in a therapeutic comprised of equal amounts of biomass from each of the spirulina strains expressing these three proteins. TcdB1 was titrated from 0 to 100 pM, and at each concentration of TcdB pilot study information was used to solve Equation 2 for VHH concentrations that were predicted to normalize scaled viability scores to 80%, with a

cap of 5 nM total VHH, assuming independent binding of the VHHs. An alternative hypothesis was also considered, where the VHHs competitively bound TcdB.

The 80% target was selected so that less inhibition than predicted would fall into the dynamic range of the assay, thus allowing deviations from independent binding to be quantitated. Design of Experiments (DoE) literature refers to this approach as model-based design, optimized for rejecting the independent binding hypothesis. That is, the conditions of the assay were selected such that most of the data would fall into the assay's dynamic range if independent binding occurred, and show (much) lower fractional viability if competitive binding occurred.

Singleton pp1005 recovered ~75% viability up to ~0.01 pM TcdB, while pp1006 and pp1007 showed low recovery at all concentrations (Fig. 1B). Binary 1:1 molar ratio mixtures of all pairs recovered ~75% viability through 0.1 pM TcdB, or less if pp1005 was not part of the mixture (Fig. 1C). Trinary mixes, with the same 5 nM total concentration cap (1:1:1 and 1:5:7) were the only cases where viability recovery was possible across most of the TcdB concentration range (Fig. 1D).

These data support the independent binding model, and we emphasize that this comparison is essential for optimal development of antibody cocktails. Model selection (independent or competitive) was performed by using the Schwarz's Bayesian criterion (BIC) (*32*), goodness-of-fit diagnostics, and the requirement that all model parameters be significant at the $p<0.1$ level. The independent model (BIC=-714) was strongly preferred over the competitive model (BIC=-273). (*25–27*). The competitive model cannot adjudicate the extremely potent triple cocktails and lower potency singleton and dual agents with the additive/competitive assumption (fig. S3).

The synthetic activity of a drug combination can be quantified by expressing the potency (EC_{50}) of a cocktail as if it were a single agent, to allow comparison to alternative single agent interventions. In this

example, EC_{50} is defined as the concentration of VHH that shifts TcdB potency 2-fold (α=2) per Equation 4. Table 1 provides these calculations for two or more binders. In the context of a clinically relevant 20 ng/mL TcdB concentration the fold-shift, α, required to recover 50% cellular viability (IC_{50}) is 58,500 - fold. For a single antibody, this means that the ratio of concentration to EC_{50} must be 58,500. For an antibody, such as pp1007 with an EC_{50} of 69.3 pM, this requires a concentration of 4.05 μM.

In contrast, a 1:1:1 molar ratio of pp1005: pp1006: pp1007 would require 6.35 nM to recover 50% viability (a synthetic EC_{50} of 109 fM) a 638 -fold reduction relative to the single antibody. A more optimal 1:5:7 molar ratio of pp1005: pp1006: pp1007 would require 4.66 nM to recover 50% viability, (a synthetic EC_{50} of 79.7 fM) an 869-fold reduction relative to the single antibody. This provided robust in vitro neutralization across the very wide range of TcdB concentrations found in patients with CDI (*23*) (Fig. 1).

To generalize this key finding, equation 4 can be expanded. As an example, assuming a 5 nM total antibody concentration and a target of 50% cell viability (α=58,500), the potency of a single agent would need to be almost 1,500-fold greater than the individual components of a cocktail of 5 independent, equally potent binders (8.5 fM vs. 0.1253 nM). To recover 80% cell viability the required potency of a single binder would be 3,000-fold greater than the components of a cocktail of 5 binders, and to recover 99% viability the relative potency would be 13,400-fold. This approach can be applied to alternative total binder concentrations, number of binders, differing binder concentrations and potencies, and differing fold-shift targets.

Genome sequences of *C. difficile* clinical isolates have been used to define 12 distinct TcdB groups (*33*). 96% of the TcdB genes present in that dataset belong to groups 1, 2, 3, and 5 (*22*, *34–36*). Consistently with the high degree of conservation of the VHH binding sites (*28*) each VHH homodimer exhibited

strong neutralizing activity against all tested toxin types except pp1005, which was only weakly active against toxin type 5. (Fig. 2). The triple VHH cocktail potently neutralized all tested toxin types relative to bezlotoxumab whose neutralizing activity against toxin type 2 (ribotype 027) was notably weak.

We used response surface methodology to select the optimal antibody ratio. In the general case of independent binding where the potencies of each component differ, there exists a unique set of fractions of binders that maximize α.

Equation 4 was used to simulate TcdB IC_{50} fold-shift (α) as a function of total VHH concentration and all combinations of fractions of pp1005, pp1006, and pp1007 summing to 1.0. The optimal mixture varies by total VHH concentration and/or total TcdB concentration. When the concentrations of VHHs are lower than the potency estimates of pp1006 and pp1007, overweighting pp1005 in the mixture is optimal (Fig. 3A and fig. S4). When the ratio of VHH concentrations to their potency exceeds 1.0, the geometric advantage of synthetic activity results in a mixture of VHHs (Fig. 3B). When the concentrations of VHHs are greater than the potency estimates, pp1005 effect saturates at E_{max}=45.25 fold and so overweighting pp1006 and pp1007 is more effective (Fig. 3, C and D). Supplemental Figure S4 presents a concise summary of optimal mixtures across a range of total VHH concentrations.

At a clinically relevant TcdB concentration of 20 ng/mL and a total VHH concentration of 10 nM, the optimal VHH mixture was determined to be 1.8%, 49.2% and 49.0% pp1005, pp1006 and pp1007, respectively. This would inhibit 92% of the TcdB effect. The saturating nature of pp1005 implies a very small fraction of pp1005 is needed at these high VHH concentrations, and the remainder of the mixture should be made up of pp1006 and pp1007 that do not saturate in effect.

An orally delivered *C. difficile* therapeutic, LMN-201, was manufactured using the edible microorganism spirulina (*Arthrospira platensis*) as the expression and delivery platform for the 3 VHHs described here (fig. S5-7) (*29*). In addition, LMN-201 also included a fourth spirulina strain expressing the catalytic domain of the bacteriophage PlyCD endolysin, which is specific for *C. difficile* (*37–39*). We reasoned that efficacy would be enhanced by inclusion of a phage-derived endolysin that destroys the *C. difficile* bacterium. Expression levels were 0.5%, 2.3% and 3.4% of dry biomass for dimeric 5D, E3 and 7F, respectively, and 0.5% for the lysin (fig. S6A). The bioactivity of the lysin component of LMN-201 was confirmed by *C. difficile* killing (fig. S7C). Importantly for oral delivery, the four therapeutic proteins all demonstrated substantial resistance to degradation by three common intestinal proteases: trypsin, elastase, and chymotrypsin (fig. S8 and fig. S9). Assembling equal amounts of each spirulina strain into the final cocktail builds a therapeutic with VHH ratios of 1:5:7 (8.1%, 37.1% and 54.8% pp1005, pp1006 and pp1007), which closely approximate the ideal dose ratios described above, with a predicted 90% inhibition of 20 ng/mL TcdB effect at a total VHH concentration of 10 nM.

Animal challenge models were used to assess efficacy *in vivo*. Cohorts of male C57BL/6J mice (*17*) were infected with *C. difficile* spores 24 hours after administration of: vancomycin (positive control); wild-type spirulina (negative control); Cocktail 1, spirulina biomass containing the three VHHs plus the lysin; or Cocktail 2, which omitted the lysin. Each treatment was administered by oral gavage once daily (fig. S10 and tables S2 and S3). Cocktail 1 significantly reduced fecal spore shedding, and decreased challenge-associated weight loss. Treatment with the Cocktails 1 and 2 also increased survival rates, with borderline significance (p=0.08) as expected from the binary nature of the survival endpoint.

For the Golden Syrian Hamster model (*40*) we compared mice treated with control wild-type spirulina biomass to mice treated with spirulina biomass containing anti-TcdB VHHs (3) + Anti-TcdA VHHs (2) +

lysin PlyCD. Each treatment was administered twice daily by oral gavage (fig. S11). Anti-TcdA VHHs were included because TcdA contributes significantly to disease in hamsters (*10*). The therapeutic cocktail significantly extended mean survival time compared to the wild-type spirulina control, and significantly reduced *C. difficile* colonization of the cecum.

The results here provide a paradigm for developing highly potent cocktail-based interventions against diseases refractory to single-therapeutic approaches. The extreme potency of a drug combination is the result of the laws of mass action governing the independent interactions of its components with a common target. Collectively, these interactions mimic a single ultra-potent agent. For the specific case of an antibody cocktail its potency can be expressed as if it were a single high avidity antibody. Hence, we suggest the term *synthetic avidity* to represent, with a single value, the geometrically increased functional strength of an antibody combination due to multiple underlying, independent binding interactions. This is to be distinguished from the more common use of avidity to describe an apparent affinity increase resulting from dependent binding interactions. We further show how response surface methodology can be used to optimize the ratios of the cocktail components, with results that depend critically on their relative potencies and the concentration of the target. These approaches may also be useful for developing drug cocktails that are highly potent activators of specific pathways, such as those that promote apoptosis.

In conclusion, the efficacy of conventional monotherapies can be vastly improved by cocktail therapeutics. As illustrated here, one application would be when the degree of target inactivation necessary for clinical efficacy is unachievable by a single agent. Also, by allowing equal or greater on-target potencies at lower drug doses, cocktail therapeutics can mitigate the dose-limiting off-target toxicities that are often problematic for monotherapies. Lastly, we highlight that ultra-potent therapeutic combinations may buffer

against decreased efficacy due to target variation, for example when treating infectious diseases or genetically unstable cancers.

References and Notes

1. G. M. Keating, *Drugs*. 75, 675–685 (2015).

2. R. D. Moore, R. E. Chaisson, *Aids*. 13, 1933–1942 (1999).

3. T. Einav, J. D. Bloom, *Plos Comput Biol*. 16, e1007830 (2020).

4. E. Balsells *et al.*, *Journal of Global Health*. 9, 010407 (2019).

5. J. G. Bartlett, *N. Engl. J. Med.* 376, 381–382 (2017).

6. M. H. Wilcox *et al.*, *N. Engl. J. Med.* 376, 305–317 (2017).

7. D. Seal *et al.*, *Eur J Clin Microbiol*. 6, 51–53 (1987).

8. S. A. Kuehne *et al.*, *Nature*. 467, 711–713 (2010).

9. D. Lyras *et al.*, *Nature*. 458, 1176–1179 (2009).

10. K. Chen *et al.*, *Sci Transl Med*. 12, eaax4905 (2020).

11. L. V. Aelst, M. Symons, *Genes & Development*. 16, 1032–1054 (2002).

12. N. Schlegel, M. Meir, V. Spindler, C.-T. Germer, J. Waschke, *J Cell Physiol*. 226, 1196–1203 (2011).

13. R. Pradhan, P. A. Ngo, L. D. Martínez-Sánchez, M. F. Neurath, R. López-Posadas, *Cells*. 10, 66 (2021).

14. G. P. Carter *et al.*, *mBio*. 6, e00551 (2015).

15. S. J. Mileto *et al.*, *Proceedings of the National Academy of Sciences*. 117, 8064–8073 (2020).

16. S. D. Bella, P. Ascenzi, S. Siarakas, N. Petrosillo, A. di Masi, *Toxins (Basel)*. 8, 134–25 (2016).

17. M. L. Hutton *et al.*, *Sci. Rep.* 7, 16020–13 (2017).

18. J. Steele, J. Mukherjee, N. Parry, S. Tzipori, *J. Infect. Dis.* 207, 323–330 (2012).

19. A. B. Ryder *et al.*, *J Clin Microbiol*. 48, 4129–4134 (2010).

20. N. R. Pollock, *Journal of Clinical Microbiology*. 54, 259–264 (2016).

21. H. Hamidi, J. Lilja, J. Ivaska, *Bio-protocol*. 7 (2017), doi:10.21769/bioprotoc.2646.

22. E. Shen *et al.*, *Commun Biology*. 3, 347 (2020).

23. C. D. Alonso *et al.*, *Clin Infect Dis*, ciab826- (2021).

24. B. D. Navalkele, T. Chopra, *Biologics Targets Ther*. 12, 11–21 (2018).

25. D. K. Shah, A. M. Betts, *mAbs*. 5, 297–305 (2013).

26. Z. Yang *et al.*, *J. Infect. Dis.* 210, 964–972 (2014).

27. D. J. Schmidt *et al.*, *Clinical and Vaccine Immunology*. 23, 774–784 (2016).

28. P. Chen *et al.*, *Nat Struct Mol Biol*. 26, 712–719 (2019).

29. B. W. Jester *et al.*, *Nat Biotechnol*, 1–9 (2022).

30. P. P. Burgers *et al.*, *FEBS J*. 283, 2132–2148 (2016).

31. J. Meador, R. K. Tweten, *Infect Immun*. 56, 1708–1714 (1988).

32. *Akaike information criterion statistics* (reidel, 1987), vol. 29 of *Mathematics and Computers in Simulation*.

33. M. J. Mansfield *et al.*, *PLoS Pathog*. 16, e1009181 (2020).

34. I. A. Tickler *et al.*, *Anaerobe*. 60, 102050 (2019).

35. A. Y. Guh *et al.*, *N. Engl. J. Med.* 382, 1320–1330 (2020).

36. Z. Li *et al.*, *Front Microbiol*. 11, 1310 (2020).

37. Q. Wang, C. W. Euler, A. Delaune, V. A. Fischetti, *Antimicrobial Agents and Chemotherapy*. 59, 7447–7457 (2015).

38. V. A. Fischetti, *Current Opinion in Microbiology*. 11, 393–400 (2008).

39. Z. Peng *et al.*, *Front. Microbio.* 9, 3234 (2018).

40. A. K. Roberts *et al.*, *Front Microbiol*. 11, 578903 (2020).

41. G. Yang *et al.*, *Bmc Microbiol*. 8, 192 (2008).

42. F. W. Studier, *Protein Expres Purif*. 41, 207–234 (2005).

43. J. J. Moré, *Lect Notes Math*, 105–116 (1978).

44. S. Raran-Kurussi, D. S. Waugh, *Plos One*. 7, e49589 (2012).

45. J. Hanoune, N. Defer, *Annu. Rev. Pharmacol. Toxicol.* 41, 145–174 (2001).

Acknowledgments: We thank Charles Shoemaker, George McDonald, Fred Cross, Barry Stoddard, and Robert Benezra for help, discussion, and advice. We thank Meagan James and other members of the Lyras laboratory for help with the mouse studies. For the hamster challenge studies we thank Sangun Lee, Christian Gonzalez and Ryan Ranallo for their efforts.

Funding: Lumen Bioscience has utilized the non-clinical and pre-clinical services program offered by the National Institute of Allergy and Infectious Diseases to perform the hamster challenge studies.

Authors contributions:
M.T., M.D., N.K, and J.M.R. conceived of the idea. M.T., H.Z., M.D., M.G., K.K., A.P., B.W.J., D.L., V.F., and M.D. developed methodologies. H.Z., M.D., M.T., M.G., K.K., B.J., M.H., A.P., H.T., T.P., S.J.M., R.H., D.L., A.M., M.Z., S.E., C. Brady, N.S., K.C., S.S., J.D., T.S., C.S., D.F., K.S., and L.G. conducted investigations. M.D., H.Z., M.G., B.W.J., H.T., C.G., and K.K. performed formal analysis. N.K., C.A.Behnke., J.M.R., and B.F. acquired funding for the project. N.K. and J.M.R. administered the project. H.Z., M.D., M.G., K.K, B.W.J., M.H., H.T., S.J.M., R.H., D.L., V.F., and J.M.R. contributed to the writing the original manuscript draft. M.D., H.Z., N.K., and J.M.R. reviewed and edited the final draft. The project was supervised by J.M.R.

Competing interests: J.R. and B.F. are the founders and current employees of Lumen Bioscience, Inc. (Lumen) and own stock/stock options in Lumen. H.Z., M.D., M.G., A.M., K.K., A.P., B.W.J., N.K., M.Z., S.E., C.Brady, M.H., H.T., T.P., S.S., J.D., T.S., C.S., D.F., K.S., C.G., V.F. and C.A.Behnke are current employees or paid advisors of Lumen; all current and former employees own stock/stock options of Lumen. M.T., N.S., K.C. and L.G. were employees of Lumen at the time of data generation. The other authors declare no competing interests. Lumen has issued patents (US Patent Nos. 10,131,870, 10,415,012, 10,336,982, 10,415,013) and pending patent applications (U.S. Patent Applications 17/245,837 and 16/570,520 and International Application no. PCT/US2020/040794) relating to certain research described in this article. Lumen has licensed U.S. Patent Nos. no. 9,834,616 and 11,091,563 and U.S. Patent Application No. no. 17/371,762 from Tufts University.

Data and materials availability: The materials developed in this study can be provided by Lumen Bioscience pending scientific review and a completed material transfer agreement. Requests for material should be submitted to J.M.R. The datasets generated during and/or analyzed during the current study are available from the corresponding author upon reasonable request.

Supplementary Materials:

Materials and Methods

Supplementary Text

Figs. S1 to S11

Tables S1 to S3

Model	Exclusive/Competitive Binding	Simultaneous/Independent Binding
Stoichiometry	$A + T \overset{K_A}{\leftrightarrow} AT$ $B + T \overset{K_B}{\leftrightarrow} BT$	$A + T \overset{K_A}{\leftrightarrow} AT + B \overset{K_B}{\leftrightarrow} ABT$ $B + T \overset{K_B}{\leftrightarrow} BT + A \overset{K_A}{\leftrightarrow} ABT$
Free Fraction of Target	$f_T = \frac{1}{1 + \frac{A}{K_A} + \frac{B}{K_B}}$ general form for *N* binders: $f_T = \frac{1}{1 + \sum_{i=1}^{N} \frac{I_i}{K_i}}$	$f_T = \frac{1}{1 + \frac{A}{K_A} + \frac{B}{K_B} + \frac{A}{K_A} \cdot \frac{B}{K_B}}$ general form for *N* binders: $f_T = \frac{1}{\prod_{i=1}^{N} \left(1 + \frac{I_i}{K_i}\right)}$
Fold-Shift of Target Potency	$\alpha = 1 + \frac{A}{K_A} + \frac{B}{K_B}$ general form for *N* binders: $\alpha = 1 + \sum_{i=1}^{N} \frac{I_i}{K_i}$	$\alpha = 1 + \frac{A}{K_A} + \frac{B}{K_B} + \frac{A}{K_A} \cdot \frac{B}{K_B}$ general form for *N* binders: $\alpha = \prod_{i=1}^{N} \left(1 + \frac{I_i}{K_i}\right)$
Synthetic Activity	$K_N = \frac{A + B}{\frac{A}{K_A} + \frac{B}{K_B}}$ general form for *N* binders: $K_N = \frac{\sum_{i=1}^{N} I_i}{\alpha - 1} = \frac{\sum_{i=1}^{N} I_i}{\sum_{i=1}^{N} \frac{I_i}{K_i}}$	$K_N = \frac{A + B}{\frac{A}{K_A} + \frac{B}{K_B} + \frac{A}{K_A} \cdot \frac{B}{K_B}}$ general form for *N* binders: $K_N = \frac{\sum_{i=1}^{N} I_i}{\alpha - 1} = \frac{\sum_{i=1}^{N} I_i}{\prod_{i=1}^{N} \left(1 + \frac{I_i}{K_i}\right) - 1}$

Table 1. Differences in stoichiometry, free fraction, fold-shift of target potency and optimal mixture ratios for agents that compete for the same binding site (left column) or do not compete for the same binding site (right column). Stoichiometry reflects association-dissociation of binders (A, B) and target (T) with dissociation equilibrium constants (K_A, K_B) to form complexes (AB, BT and ABT). Free fraction follows from an expansion of Equation 3 to two or more agents. Fold-shift of target potency follows from

an expansion of Equation 4 to two or more agents. Commonly, selecting the optimal mixture in the exclusive case leads to the decision to use only the most potent agent. In contrast, the optimal mixture in the exclusive case is defined by relative potencies.

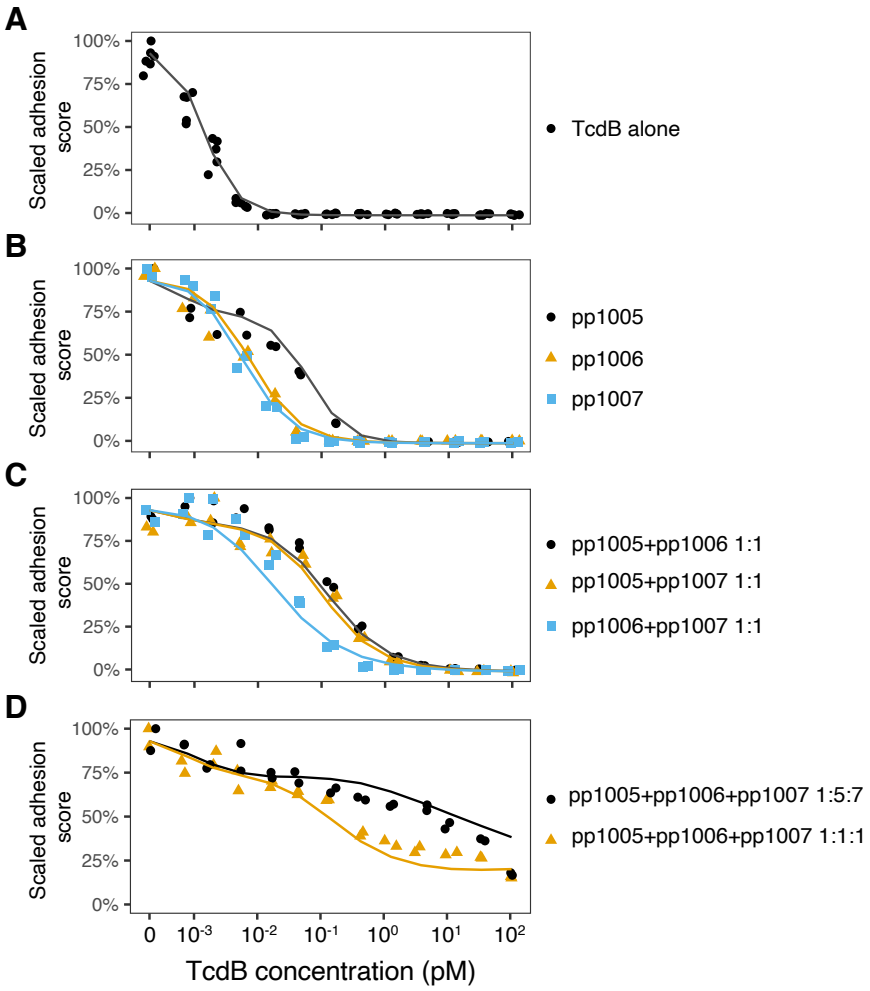

Fig. 1. Independent model fits (lines) to observed scaled viability scores (points). (**A**) TcdB alone, titrated from 0 to 100 pM. (**B**) Singleton VHHs pp1005, pp1006, pp1007. (**C**) Dual mixtures of VHHs at a 1:1 molar concentration. (**D**) Triple mixtures of VHHs at a 1:5:7 and 1:1:1 molar concentration. VHH concentrations were selected to target 80% scaled viability at each TcdB level based on pilot information, with a cap of 5 nM total VHH.

1

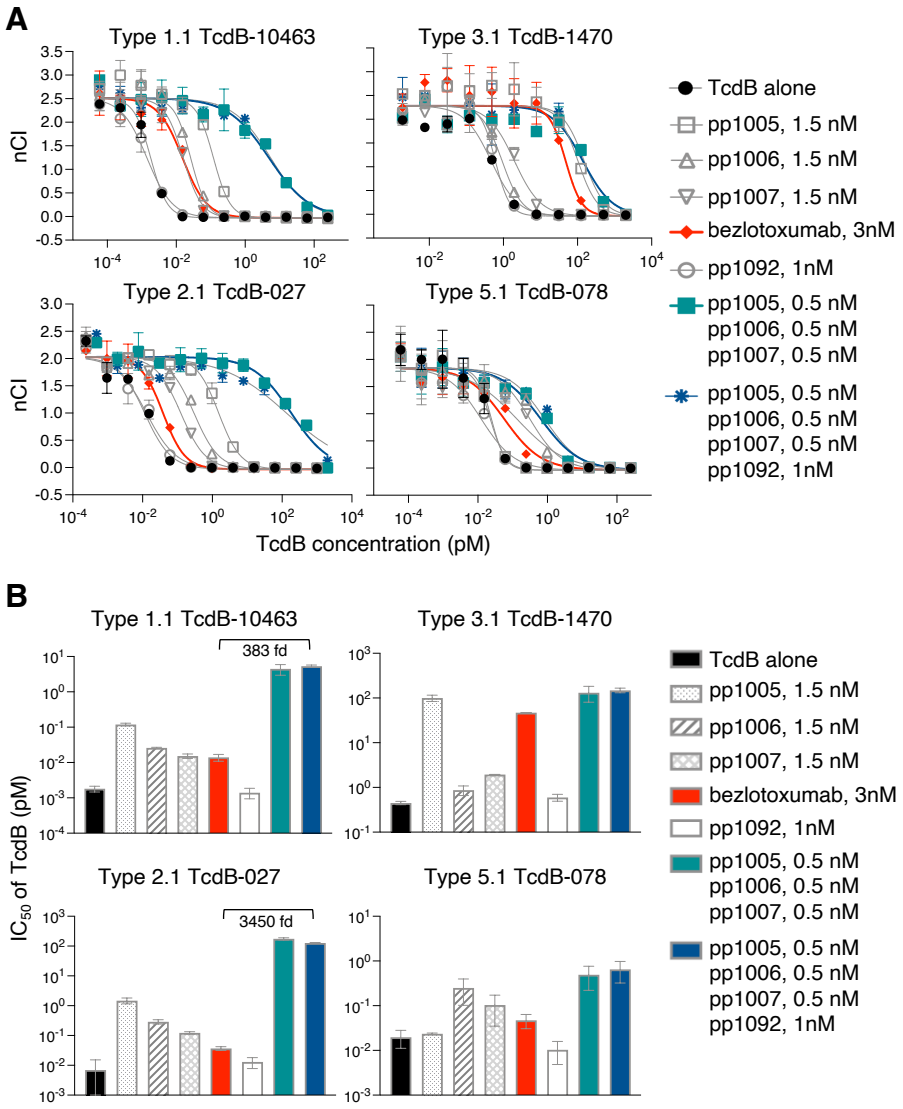

2

3 **Fig. 2. Comparative neutralization of the five major TcdB types by LMN-201 and bezlotoxumab.**

4 (**A**) Neutralizing activity of pp1005, pp1006, pp1007, and the triple cocktail on toxin types 1.1, 2.1, 3.1

5 and 5.1. 1.5 nM of each dimeric VHH or the cocktail of all three dimeric VHHs (0.5 nM of each) was

6 tested against serially diluted TcdB with Vero cells on the RTCA system. As comparison, 3 nM of

7 bezlotoxumab was similarly evaluated. To rule out interference, the effect of 1 nM lysin on VHH cocktail

8 efficacy was assessed. (**B**) IC_{50} of TcdB under treatment was calculated from the data shown in A and

9 compared.

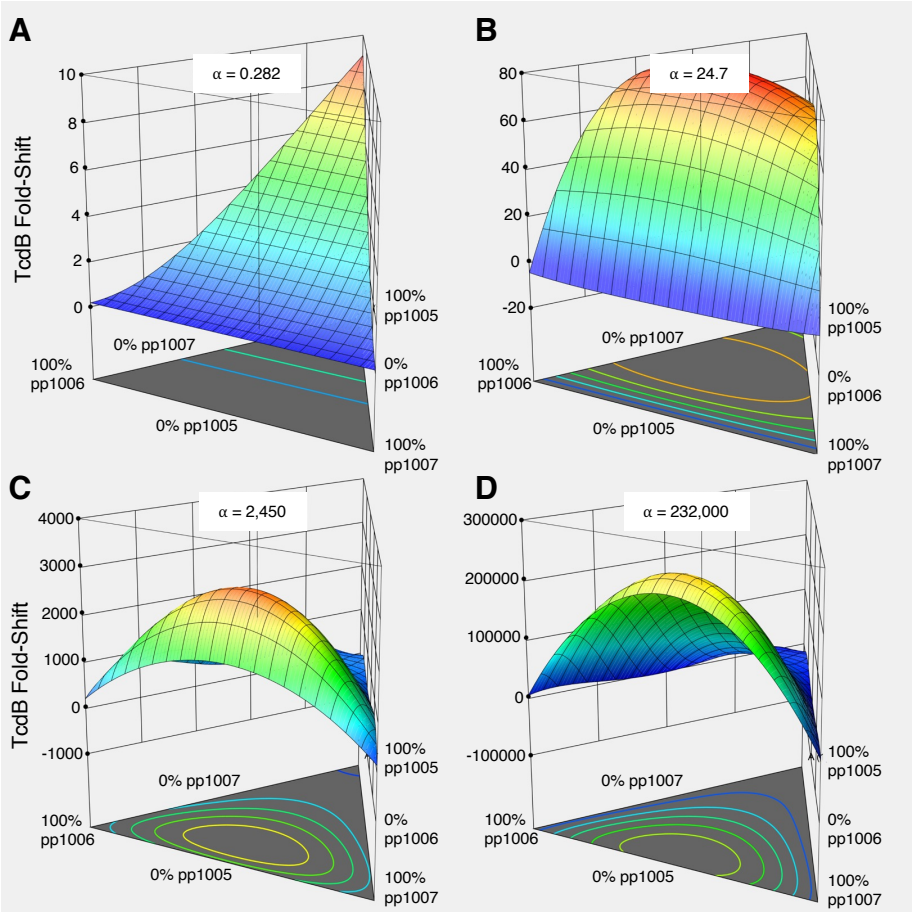

Fig. 3. Response surface diagrams for total VHH concentrations of 0.01 nM (panel A), 0.1 nM (panel B), 1 nM (panel C) and 10 nM (panel D). The ratio of pp1005, pp1006, pp1007 is 1:5:7. All possible mixtures at these concentrations were simulated, and the fold-shift (α) was calculated for each mixture condition. A (nearly) pure pp1005 mixture is optimal at 0.01 nM total VHH (panel A). As the total VHH concentration increases, greater fractions of pp1006 and pp1007 are optimal (panels B, C, D).

Supplementary Materials for

Using synthetic activity to design ultra-potent antibody cocktails

Hui Zhao[1]†, Michael Dodds[1]†, Michael Tasch[1], Mesfin Gewe[1], Anissa Martinez[1], Melanie Hutton[2], Kristie Keeney[1], Alex Pollock[1], Benjamin W. Jester[1], Nhi Khuong[1], Mia Zhang[1], Stacey Ertel[1], Colin Brady[1], Mark Heinnickel[1], Hannah Tabakh[1], Nathan Sanjaya[1], Kendra Cruickshank[1], Troy Paddock[1], Sarah Struyvenberg[1], Jason Dang[1], Tracy Saveria[1], Chelsea Shanitta[1], David Fletcher[1], Kristjan Sigmar[1], Lauren Goetsch[1], Caitlin Gamble[1], Steven J. Mileto[2], Ryan Heselpoth[3], Dena Lyras[2], Craig A. Behnke[1], Vincent Fischetti[3], Brian Finrow[1], and James M. Roberts[1,*]

Correspondence to: jroberts@lumen.bio

This PDF file includes:

Materials and Methods
Supplementary Text
Figs. S1 to S11
Tables S1 to S3

Materials and Methods

Engineering of spirulina

Spirulina strains without exogenous selection markers were generated as described (*29*). In brief, the natural spirulina gene WP_006618409.1, which confers resistance to kanamycin, was replaced with an exogenous gene encoding resistance to streptomycin to generate spirulina strain SP205. SP205 was then transformed with constructs containing the gene of interest, WP_006618409.1, as well as the homology arms. The transformants were selected with kanamycin. Single filaments were isolated and propagated to generate cell banks. DNA extracted from cells grown from the cell banks was used for PCR, Sanger sequencing and Illumina Next Generation Sequencing. Complete segregation was confirmed. Sequences of the gene of interest and WP_006618409.1 were verified.

Illumina next generation sequencing of spirulina

Spirulina genomic DNA was extracted using a Blood and Tissue Kit (Qiagen) with minor modifications. Spirulina biomass was resuspended in buffer ATL. It was digested with proteinase K (2 mg/mL) overnight at 56 °C and then treated with RNase A (10 mg/mL) for 20 minutes at 56 °C. 400 µL of buffer AL was added and the sample was centrifuged for 10 minutes at 13,000g. The supernatant was mixed with 250 µL of 100% ethanol and applied to DNeasy columns. The columns were washed once with 500 µL buffer AW1 and once with 500 µL AW2. The DNA was eluted with molecular grade water. Genomic DNA was quantified by a Qubit dsDNA High Sensitivity (HS) and Broad Range (BR) Kit (Thermo Fisher Scientific) and prepared for Illumina analysis using the Illumina DNA prep kit (Illumina). Illumina sequencing of the spirulina genome was performed on a MiSeq instrument using a MiSeq Reagent Kit v2 (Illumina).

1 Illumina analysis for copy number determination

2 Copy numbers of the genes of interest in SP1287, SP1308, SP1312, and SP1313 were determined
3 by comparing the abundance of the transgenes to 10 randomly selected genes (referred to as
4 "normalization genes": *ppaX, rpsA, chlM, degU2, radA, rbcL, sdhA, psbC, cysA1, smc6*) in the genome. A
5 copy number of about 1±0.15, was expected and set as the benchmark for a full genomic integration of 1
6 gene/genome copy. As a validation control, a second set of 10 random spirulina genes (*thrB1, hisC1,*
7 *isfD2, pilA, purB, apcE, nblA, gpmB, bicA2, cpcBA*) were compared pairwise to the "normalization genes"
8 set in a manner identical to the transgene. Gene copy number per genome was determined by first using
9 samtools (http://www.htslib.org/doc/) to generate an mpileup file with Illumina reads per base pair. The
10 median read per base pair was determined across the 10 "normalization genes" and the transgene. The
11 median read per base pair of the transgene was then divided by the 10 "normalization genes" median read-
12 per-base-pair value.

13 Expression analysis of recombinant proteins in spirulina

14 To prepare soluble extracts, dried or wet spirulina biomass was resuspended in PBS containing
15 Pierce Protease Inhibitor cocktail, EDTA-free (Thermo Scientific) and 1 mM phenylmethylsulfonyl
16 fluoride (PMSF, Thermo Scientific) at a biomass concentration of 2-10 mg/mL. The resuspended biomass
17 was applied to 0.1 mm silica beads and lysed using a Percellys Evolution homogenizer (Bertin
18 Technologies). The soluble fraction was separated by centrifugation at 15,000 g at 4 °C for 30 minutes for
19 downstream analysis.

20 Accumulation of soluble recombinant protein in spirulina was measured using a capillary electrophoresis-
21 based immunoassay with a Jess instrument (ProteinSimple) according to manufacturer's instructions.
22 Briefly, the soluble extracts were diluted (0.1-1 mg/mL biomass) using water and Master Mix

(ProteinSimple) and standard curves were generated by a titration of purified protein. Proteins were separated using a 12-230 kDa Jess/Wes Separation Module (ProteinSimple). Recombinant protein was detected by probing with a mouse anti-His-Tag primary antibody (GenScript) (1:100) followed by an anti-mouse IgG NIR fluorescence-conjugated secondary antibody (ProteinSimple). Non-reducing denaturing gels were performed in a similar manner; with reductant withheld from the 5X master mix. Data analysis was performed using the ProteinSimple Compass software and Microsoft Excel.

To prepare total cellular extracts (soluble and insoluble), spirulina biomass was resuspended in PBS with 0.02% Triton X-100 and lysed prior to homogenization as described above. Following lysis, samples were diluted to 0.1-1 mg/mL in extraction buffer (60 mM dithiothreitol, 60 mM Na_2CO_3, 6 mM ethylenediamine tetraacetic acid, 2% (w/v) sodium dodecyl sulfate, 12% (w/v) sucrose and 0.02% Triton X-100). Samples were immediately heated at 100 °C for 120 seconds, centrifuged at 16,000 g for 5 minutes, and the extracts analyzed on the Jess instrument as described above.

Protein purification from spirulina biomass

VHHs 5D (pp1005), E3 (pp1006), and 7F (pp1007), and full-length lysin PlyCD (pp1092) were purified from spray-dried spirulina biomass using Ni-NTA affinity and size-exclusion chromatography 2-step purification protocol. Dried biomass was resuspended at 30 mL/g in PBS with protease inhibitor mix as described above. Resuspended biomass was lysed using a high-pressure homogenizer (Microfluidics LM20) at 12,000 psi. The lysates were centrifuged at 18,500 *g* at 4 °C on tabletop centrifuge for 30 minutes. The resulting supernatant was filtered using a coffee filter followed by 0.22 µm membrane filter. Recombinant proteins were purified from the clarified lysate by affinity chromatography using 5 mL HisTrap columns (Cytiva) equilibrated with 50 mM Tris pH 8.0, 300 mM NaCl and 20 mM imidazole (Thermo Fisher Scientific). HisTrap-purified samples were further refined using AKTA Pure FPLC-based

size-exclusion chromatography on HiLoad 16/600 Superdex 200 pg column (Cytiva). Protein purity and sizing were assayed by size-exclusion chromatography on analytical Superdex 200 increase 10/300 (Cytiva) where 100 µL of purified protein at ~1 mg/mL was run in PBS. Purified protein samples were also assessed on SDS-PAGE under reducing and non-reducing conditions. 3 µg protein samples were incubated at 70 °C in LDS loading buffer with or without 20 mM dithiothreitol (DTT) reducing agent (Thermo Fisher Scientific). Proteins were determined to be >90% pure and exhibited the expected molecular weight size distribution.

Cell lines, bacterial strains, and toxins

Vero cells (ATCC) were cultured in Dulbecco's Modified Eagle Medium (DMEM) supplemented with 10% heat-inactivated fetal bovine serum and 1% penicillin-streptomycin (Gibco). Cells were grown in a high-humidity incubator at 37 °C and 5% CO_2. *C. difficile* toxin TcdB-10463 was expressed in *Bacillus megaterium* and purified using Ni-NTA affinity and ion exchange chromatography. Purified *C. difficile* toxins TcdB-027, TcdB-1470, and TcdB-078 were purchased from tgcBIOMICS. Bezlotoxumab was sourced from Henry Schein Medical.

Expression of recombinant TcdB toxin, inactive TcdB and TcdB subdomains in bacterial systems

Active and inactive TcdB toxin were expressed in *B. megaterium* bacteria and purified following a reported protocol with minor modifications (*41*). Transformant *B. megaterium* cells were generously provided by Dr. Charles shoemaker lab (Tufts University). Transformed bacteria from glycerol stocks were streaked on Luria broth agar (LB) plates with 10 µg/mL tetracycline. LB medium supplemented with 10 µg/mL tetracycline were inoculated with single *B. megaterium* colonies and grown overnight. Cultures were then diluted into Super Broth media (Teknova) supplemented with tetracycline and grown in a shaking incubator at 37 ^{o}C. Protein expression is induced with 0.5 % (w/v) xylose at optical density (OD_{600}) of 0.3 - 0.4. Bacterial cultures were harvested by centrifugation after 16 hours of induction. To

purify His-tagged TcdB, cell pellets were resuspended in 50 mM sodium phosphate, 300 mM NaCl, 20 mM imidazole, 0.5 mM EDTA lysis buffer at pH 8.0. Resuspended cell emulsions were lysed by sonication using amplitude of 30 with 30 second ON, interspersed with 60 second OFF for a total process time of 10 min. Cell lysate supernatant were clarified by centrifugation at 18,500 *g* at 4 °C for 20 minutes. Recombinant proteins were purified from the clarified lysate by affinity chromatography using 5 mL HisTrap columns (Cytiva) equilibrated with 50mM Tris pH 8.0, 300 mM NaCl and 20 mM imidazole (Thermo Fisher Scientific) on Akta Pure FPLC system and UNICORN software (Cytiva). His-tagged protein bound HisTrap columns were washed with 10 column volumes (CV) wash buffer (50 mM Tris, pH 8.0, 300 mM NaCl and 20 mM imidazole). Bound His-tagged protein were eluted using gradient flow at slope of 10% - 100% elution buffer (50 mM Tris pH 8.0, 300 mM NaCl and 250 mM imidazole) in 5 CV. Fractions containing the eluted protein were assessed by SDS-PAGE. Samples were diluted in NuPAGE LDS Sample Buffer (Thermo Fisher Scientific) and treated 70˚C for 10 minutes prior to analysis. Proteins were separated on Bis-Tris NuPAGE 4 to 12% gels, followed by Coomassie Blue gel staining. Fractions were pooled based on level of purity, concentrated, and further purified using ion exchange chromatography on 5 mL HiTrap QXL columns (Cytiva). Purity of the purified active and inactive forms of recombinant TcdB proteins were determined using SDS-PAGE analysis under reducing and non-reducing conditions. Fractions were pooled based on level of purity, concentrated, and buffer exchanged into PBS. Protein concentrations were determined by absorbance using a Nanodrop microvolume spectrophotometer (Thermo Scientific).

The VHH-binding domains on TcdB (*28*) were designed for bacterial expression with an N-terminal hexahistidine tag followed by MBP and TEV protease recognition site (ENLYFQG) and C-terminal Avi-tag (LNDIFEAQKIEWHE) for enzymatic biotinylation. Based on the structural information, we designed the 5D-binding region and the delivery and receptor-binding domain (DRBD) for expression

using residues from amino acid position 1092 to 1433 of TcdB. VHHs 7F and E3 bind regions on the glucosyltransferase domain (GTD). A fragment containing this region, from amino acid position 2 through 543 of TcdB, was subcloned into a modified pET28 b (+) vector where the kanamycin bacterial resistance gene was replaced with ampicillin bacterial resistance gene. Sequence verified plasmids were transformed into BL21(DE3) *Escherichia coli* cells (New England Biolabs) and plated on LB medium supplemented with 100 µg/mL ampicillin. Protein was expressed using autoinduction protocol (*42*). Briefly, 1 L of Super Broth media containing appropriate selection drug was inoculated with overnight cultures from individual transformants, shaken at 37 °C for 8 hours followed by 16 °C for 24 hours. Cells were harvested by centrifugation and the pellet stored at −20 °C until processing. Frozen pellets were thawed on ice and resuspended in 100 mL of 50 mM Tris pH 8.0, 300 mM NaCl, supplemented with a Pierce Protease Inhibitor cocktail (Thermo Scientific) and 1 mM PMSF. Cells were lysed by high pressure homogenization (12,000 psi) and the lysates were clarified by centrifugation at 18,500 *g* at 4 °C for 30 minutes. Recombinant proteins were purified from the clarified lysate by affinity chromatography using 5 mL HisTrap columns. The columns were washed with 10 column volumes (CV) of wash buffer (50 mM Tris, pH 8.0, 300 mM NaCl and 20 mM imidazole) prior to elution using gradient flow at slope of 10% - 100% elution buffer (50mM Tris pH 8.0, 300mM NaCl and 250 mM imidazole) in 5 CV. Fractions containing the eluted protein were assessed by SDS-PAGE. Samples were diluted in NuPAGE LDS Sample Buffer (Thermo Fisher Scientific) and treated 70˚C for 10 minutes prior to analysis. Proteins were separated on Bis-Tris NuPAGE 4 to 12% gels, followed by Coomassie Blue gel staining. Fractions were pooled based on level of purity, concentrated, and buffer exchanged into PBS. Samples were then filtered through a 0.2 µm filter and run over a size-exclusion column on AKTA Pure FPLC-based size-exclusion chromatography HiLoad 16/600 Superdex 200 pg column (Cytiva) equilibrated in 1X PBS. Purity and final analysis were performed using SDS-PAGE as described above. Purified samples were biotinylated using BirA biotin ligase (Avidity Inc.) at 1 µg of BirA enzyme per 10 nM of protein.

1 Assessment of VHH binding to TcdB subdomains with bio-layer interferometry (BLI)

2 BLI measurements were performed on the Octet RED96 system (Sartorius) using High Precision
3 Streptavidin (SAX) biosensors (Sartorius). Biosensors were hydrated with PBS, pH 7.4 at room
4 temperature for 10 minutes on microplate 96-well flat-bottom (Greiner). All kinetics experiments were
5 performed at 30 °C with 500 rpm agitation in the kinetics module. Biosensors were dipped into PBS
6 containing wells for 60 seconds, followed by loading with enzymatically biotinylated TcdB antigen
7 fragments at 10 µg/mL for 200 seconds to achieve ~0.6 – 1 nm response. Loading was quenched by
8 incubating biosensors in 50 µM biocytin (Sigma Aldrich) for 60 seconds. Baseline were established by
9 incubating antigen loaded biosensors in kinetics buffer (PBS + 0.02 % Tween 20, 0.1 % BSA, 0.05 %
10 sodium azide) for 300 seconds. The rate of association was measured by incubating antigen loaded
11 biosensor tips into 3-fold dilution series of monomeric (pp1239, pp1238, and pp1240 respectively) or
12 dimeric (pp1005, pp1006, and pp1007 respectively) 5D, E3, and 7F VHHs. The concentration series used
13 to determine binding kinetics of pp1238 were 93.6, 31.2, 10.4, 3.47, 1.16, and 0.36 nM. Concentrations
14 used to determine binding kinetics of pp1239 were 93.6, 31.2, 10.4, 3.47 and 0.38 nM. Concentrations
15 used for pp1240 were 92.2, 30.7, 10.2, 3.41, 1.14 and 0.38 nM. pp1005 was assayed at 16.2, 5.39, 1.8,
16 0.60, 0.20 and 0.07 nM. Concentrations used for pp1006 were 16.8, 5.6, 1.87, 0.62, 0.21, and 0.07 nM.
17 pp1007 were assayed at concentrations of 84.9, 28.3, 9.43, 3.14, 1.05 and 0.35 nM. Analyte bound
18 biosensors were dipped into kinetics buffer for 300 - 600 seconds to measure rate of dissociation. Kinetic
19 analysis was performed using the HT 11.1.1.39 Data Analysis module (Sartorius). Results were double
20 referenced. Both association and dissociation steps were used in 1:1 binding model global data fitting
21 model.

22 BLI methods using SAX coated Biosensors (Sartorius) was used to study epitopes and tandem
23 binding of TcdB targeting VHHs designed as dimers for spirulina expression. Recombinant, inactive TcdB

was biotinylated using EZ-Link™ NHS-Biotin (Thermo Fisher Scientific) following the manufacturers protocol at 1:3 protein to biotin ratio. Biosensors were hydrated in PBS, pH 7.4 at room temperature for 10 minutes before experiments were performed at 30 °C with 500 rpm agitation in the kinetics module. Biosensors were dipped into PBS containing wells for 30 seconds, followed by loading with biotin conjugated inactive TcdB antigen 5 µg/mL for 200 seconds to achieve ~0.6 – 1 nm response. Loading was quenched by incubating in 50 µM biocytin (Sigma Aldrich) for 30 seconds. Baseline were established by incubating antigen loaded biosensors in kinetics buffer (PBS + 0.02 % Tween 20, 0.1 % BSA, 0.05 % sodium azide) for 120 seconds. Binding response by the first spirulina expressed and purified dimeric VHH, biosensors were incubated in wells containing saturating amount (2 µg/mL) of VHH1 for 300 seconds. Biosensors were then moved to wells containing saturating amount (2 µg/mL) of VHH2 for 300 seconds. To measure simultaneous binding of all VHHs, antigen loaded and VHH1 and VHH2 bound biosensors were incubated in wells containing saturating amount (2 µg/mL) of VHH3 for 300 seconds. Binding was measured as a function of increase in response. All possible 9 combination of VHH1, VHH2 and VHH3 were tested. Response as measured in wavelength shift in nM was plotted using PRISM software (GraphPad).

Toxin neutralization assay

Toxin-neutralization assays using TcdB1.1, TcdB2.1, TcdB3.1 and TcdB5.1 were performed using the Agilent xCELLigence Real-Time Cell Analysis (RTCA) MP instrument. Cell health was measured in real-time using this impedance-based platform. Cellular adherence to a biosensor containing 96-well plate (E-plate) impedes the electron flow between the electrodes. Changes to impedance are used to calculate the cell index (CI), a unitless measurement, that is used as a readout for cellular physiology. TcdB induces cell detachment that was monitored by changes in CI.

Agilent 96-well E-plates were seeded with 1 x 10^4 Vero cells/well in 100 µL DMEM culture medium with 10% FBS and 1% Pen/Strep. After settling for 30 minutes at room temperature, plates were placed into the xCELLigence MP instrument in a CO_2 37 °C incubator (Caron) and CI was measured every 15 minutes for 20 to 24 hours. TcdB was serially diluted and incubated at 37 °C for 1 hour with purified VHH homodimer, lysin, and bezlotoxumab. The xCELLigence MP instrument was paused while culture medium was carefully removed from the E-plates. 100 µL of the protein/TcdB mixture was added to the cells in each well and the RTCA was resumed to run for at least 24 hours. CI measurements at 24-hour treatment for each well were normalized by the CI at the last reading before treatment was added. The normalized cell index (nCI) was plotted with GraphPad Prism and a nonlinear regression analysis was performed to calculate the IC_{50} of TcdB under treatments.

TcdB's effect on cell adhesion and inhibition of TcdB by anti-TcdB VHH homodimers

Toxin neutralization assay data were imported, normalized, and analyzed using R (version 4.1.1 The R Foundation for Statistical Computing). Nonlinear regression was performed using the *minpack.lm* routine in the *nlsLM* package, which implements the Levenberg-Marquardt algorithm to perform bounded minimization (*43*).

Lysin activity assay

The lytic activity of pp1092 against *Bacillus subtilis* SL4 was assessed based upon previously described methods with modifications to adapt the assay to a 96-well plate format (*37*). Mid-log phase grown SL4 in BHI (37 °C, 250 rpm) were harvested and washed twice with PBS by centrifugation (room temperature, 6,000 x g, 10 minutes). Bacteria were combined with 1µg digested or undigested pp1092 in a final volume of 200 µL at OD 1.0 and cultured at 37 °C with shaking. Turbidity reduction was measured over time. Each unknown was fit along with 5 3-fold serial dilutions of undigested standards using a modified 5-parameter nonlinear logistic model. The time of 50% OD_{600}, TC_{50}, was estimated as a 4-

parameter nonlinear logistic model with lysin concentration as the independent variable. Standard curves were generated by linear regression analysis with Excel. All results were expressed as the mean ± standard deviation as calculated by Excel. EC_{50} values were calculated using GraphPad Prism.

VHH homodimer protease digestion for ELISA and neutralization assays

In vitro protease digestions of anti-*C. difficile* VHH homodimers were prepared in a matrix of soluble lysate from wild-type spirulina (SP003) in Bis-Tris buffer pH 6.0 and treated with trypsin (Sigma), chymotrypsin (Sigma), or elastase (MP Biomedicals). VHH homodimers in PBS were diluted in SP003 lysate, Bis-Tris buffer, and protease so that the final concentrations were VHH homodimer, 20 mg/mL of SP3 lysate, and a "fed" or "fasted" amount of protease. This level of SP003 lysate and VHH homodimer simulates an expression level of 1% in spirulina (by dry weight). For trypsin and chymotrypsin, the "fed" and "fasted" levels of protease in the digestion reactions were 0.1 and 0.01 mg/mL, while for elastase, 5 and 0.5 μg/mL were used respectively. Samples were incubated at 37 °C for 1 hour with shaking at 900 rpm in an Eppendorf ThermoMixer. Reactions were quenched with an equal volume of stop buffer containing 2 mM PMSF and 2x Pierce Protease Inhibitor cocktail in PBS; elastase digests were additionally neutralized with a 1 mM elastase inhibitor III (EMD Millipore Corp). The final concentration of each VHH homodimer after protease neutralization was 0.1 mg/mL. Samples were kept on ice until ELISA or cell viability analysis.

VHH homodimer quantitation by ELISA

Digested VHH homodimers were analyzed for binding activity via ELISA. Thermo Scientific Nunc ELISA plates were coated with 100 μL/well of inactive TcdB at 2 μg/mL in CBC binding buffer and incubated overnight at 4 °C. Plates were washed 3 times with PBS supplemented with 0.05% Tween-20 (PBS-tw), then blocked for 1 hour with 300 μL/well of block (PBS-tw supplemented with 5% BLOTTO). Dilutions of undigested and digested VHH homodimer were prepared in a low-binding 96-well plate by

serially diluting with block. 6 dilutions of each undigested VHH homodimer were prepared for a standard curve. Two dilutions of each protease digested sample were prepared for quantification by interpolation from the standard curve. A 100 µL sample of each VHH homodimer was added to ELISA plate wells and incubated for 1 hour at room temperature on a plate shaker. The plates were washed as before. An HRP-conjugated anti-camelid VHH antibody cocktail (Genscript) was diluted 50,000-fold in block and 100 µL/well was added to the ELISA plates for 50 minutes with shaking. Plates were washed 2 times with PBS-tw and 1 time with PBS. Finally, 100 µL/well of TMB Ultra ELISA substrate (Thermo Fisher Scientific) was added to each well. The plates were developed in the dark at room temperature on a plate shaker for 10 minutes before being quenched with 50 µL of 2.5 M sulfuric acid, and the absorbance was read at 450 nm with a SpectraMax M5 plate reader. All digestion reactions were in duplicate, in 3 independent experiments.

Calculation of VHH homodimer protease resistance

The concentration of VHH homodimer in the protease-digested samples was calculated by interpolating the concentration from standard curves generated with undigested VHH homodimer. The percentage of remaining VHH homodimer activity after digestion was calculated by dividing the interpolated value by the amount present if no VHH homodimer were digested. Each replicate was calculated separately, and the average and standard deviation were determined across all replicates.

Toxin neutralization assay of digested VHH homodimers

Chymotrypsin-digested pp1005, pp1006, and pp1007 were assessed for toxin-neutralizing activity as described. The final concentration of pp1005, pp1006, and pp1007 was 0.05 nM, 5 nM, and 5 nM respectively and the TcdB was 1:5 serially diluted starting at 250 pM.

1 Lysin protease digestion and quantification

2 In digestion buffer (20 mM Tris, 150 mM NaCl, 3 mM $CaCl_2$ at pH 6.4), 0.2 µg/µL protein was
3 mixed with trypsin (Promega), chymotrypsin (MP Biomedicals), and elastase (MP Biomedicals) at 0.1 and
4 0.01 mg/mL and incubated at 37 °C with shaking at 200 rpm. After incubation for 1 hour, reactions were
5 immediately quenched by addition of 1 mM PMSF and 1X Pierce Protease Inhibitor Mini Tablets, EDTA-
6 free (Thermo Fisher Scientific). For samples with elastase, 1 mM elastase inhibitor III (Millipore Sigma)
7 was added as well. To visualize digestion, 2 µg of digested and undigested proteins were displayed in a
8 gradient BOLT-PAGE gel at 200 V for 20 minutes and stained with Coomassie. Pixel intensity of
9 Coomassie stained proteins were measured using ImageJ software, normalizing all bands to the undigested
10 band for each condition after subtracting background pixel intensity of an identically sized bounding box.

11 Preparation of *C. difficile* spores for mouse study

12 *C. difficile* strain M7404, a ribotype 027 clinical isolate from Canada, was cultured on HIS-T agar
13 (3.7 % (w/v) heart infusion (HI) (Oxoid), 0.5 % (w/v) yeast extract, 1.5 % (w/v) agar supplemented with
14 0.375 % (w/v) glucose, 0.1 % (w/v) L-cysteine and 0.1 % (w/v) sodium taurocholate (New Zealand
15 Pharmaceuticals)) in an anaerobic chamber (Don Whitley Scientific) with an atmosphere of 10 % H_2, 10
16 % CO_2 and 80 % N_2 at 37 °C. To prepare spores, strains were sub-cultured on HIS-T agar and inoculated
17 into 500 mL tryptone yeast (TY) broth (3.0% tryptone, 2.0% yeast extract, and 0.1% sodium thioglycolate)
18 and grown anaerobically at 37 °C for 10 days. Spores were harvested by centrifugation at 10,000*g* for 20
19 minutes at 4 °C and washed 5 times with chilled distilled water prior to heat-shocking at 65 °C for 20
20 minutes and quantified by plating onto HIS-T agar. Spores were adjusted to 10^6 CFU/mL in PBS
21 containing 0.05 % Tween-80 in preparation for mouse infections.

Mouse study design

Animal handling and experimentation was performed in accordance with Victorian State Government regulations and approved by the Monash University Animal Ethics Committee (Monash University AEC no. 21731). Male C57BL/6J mice, 6-7 weeks old, were assigned to either a spirulina therapeutic treatment group, positive control (vancomycin-treated), or negative control (wild-type spirulina-treated) group and caged in groups of 5. To induce susceptibility to *C. difficile*, the animals were pre-treated with an antibiotic cocktail in the drinking water containing kanamycin (0.4 mg/mL), gentamicin (0.035 mg/mL), colistin (850 U/mL), metronidazole (0.215 mg/mL), vancomycin (0.045 mg/mL), and cefaclor (0.3 mg/mL) for 7 days, followed by 4 days of cefaclor (0.3 mg/mL) alone. Starting 1 day prior to infection (day -1), the animals were orally gavaged with 200 µL of treatment once daily for the first two days (peak of infection) and then 100 µL once daily for the remainder of the study. Mice were infected with 10^5 spores/mouse by oral gavage.

The spirulina treatments and controls were resuspended in PBS (5% w/v) by mixing up and down using an 18G blunt needle and 1 mL syringe for 2.5 minutes and administered within 10 minutes of preparation. Vancomycin was diluted to 6.25 mg/mL prior to administration. On the day of *C. difficile* infection (day 0), antibiotic pre-treatment was ceased, the mice were switched to plain water, and infection was initiated 3 hours after the treatment dose. Mice were monitored daily for signs of infection, including weight loss, and were euthanized upon losing 15% body weight, if they reached pre-defined clinical endpoints as required by ethics, or at the end of the study (day 4). As a surrogate assessment of colonization, fecal samples collected at 24 hours post-infection and then again at the time of euthanasia were analyzed to enumerate the shedding of *C. difficile* spores. Subjects treated with a spirulina therapeutic cocktail were compared to the cohort administered wild-type spirulina.

Quantification of spore shedding from mouse feces

Fecal pellets were collected 24 hours post-infection and at time of euthanasia, resuspended in PBS (100 mg/mL), heat shocked (30 minutes, 65 °C) and plated for spore enumeration onto HIS agar supplemented with 0.1% (w/v) L-cysteine, 0.1% (w/v) sodium taurocholate, 0.375% (w/v) glucose, 250 µg/mL D-cycloserine, 8 µg/mL cefoxitin, and 10 µg/mL erythromycin.

Analysis of colonization data was performed by fitting linear models of $\log_{10}$ CFU/g data per landmark time with treatment as a (potential) explanatory factor. A coefficient for wild-type spirulina describes the mean $\log_{10}$ CFU/g for that treatment, and coefficients for each other treatment describes the difference in mean $\log_{10}$ CFU/g for that treatment relative to wild-type spirulina. Standard errors of estimates were reported, along with t-statistics and 2-tailed p-value corresponding to the t-statistic with $\alpha=0.05$.

Analysis of clinical outcomes-mouse study

Analysis of maximum weight loss data was performed by fitting linear models of maximum weight loss data with treatment as a (potential) explanatory factor. A coefficient for wild-type spirulina describes the mean maximum weight loss for that treatment, and coefficients for each other treatment describes the difference in mean loss for that treatment relative to wild-type spirulina. Standard errors of estimates were reported, along with t-statistics and 2-tailed p-value corresponding to the t-statistic with $\alpha=0.05$.

Analysis of survival data was performed on tabulated number at risk and number of events at each time. Data was compared for each treatment to wild-type spirulina results and a p-value was computed using the log-rank statistic for each comparison.

Hamster study challenge agent preparation and confirmation

C. difficile strain R20291 (NAP1/BI/027) spore stock was titered on TCCFA plates after a 30-minute incubation at 65 °C and determined to be 5 x 10^5 cfu/mL in a volume of 5 mL of PBS. This spore

stock was diluted to 15,000 spores/50 µL and further diluted in an equal volume of sterile PBS containing 5% sucrose to facilitate administration of 15,000 spores in 100 µL per animal.

To verify challenge doses, 100 µL of inoculum were serially diluted (10-fold dilutions) and plated onto TCCFA plates. After incubation of the plates under anaerobic conditions at 37 °C for 48 hours, the number of colonies were enumerated, and the doses calculated based on these numbers. The inoculum was measured to be 15,000 CFU.

Hamster study design

Hamsters (Envigo, Indianapolis, IN) were visibly checked upon arrival and allowed to acclimate to their new environment for 2 days. Each animal was given a physical exam and randomly assigned (adjusting only to distribute body weight evenly) to 1 group. They were fed *ad libitum* with sterilized 2018S Teklad Global 18% Rodent Diet (Envigo, Indianapolis, IN) and sterile water provided in standard bottles with sippers during the study. To sensitize the animals to *C. difficile* infection, clindamycin, 15 mg/mL in saline, was administered intraperitoneally at 30 mg/kg, once a day, for 3 consecutive days. During clindamycin treatment, cage bottoms were changed daily for 3 consecutive days beginning on the first day to prevent bacterial recolonization from coprophagy.

Supplementary Text

Spirulina strain engineering

VHHs 5D, E3 and 7F were expressed in spirulina strains SP1308, SP1312 and SP1313, respectively. The primary structures of each monomer subunit in the VHH homodimers were similar. From amino to carboxy terminus this was: the maltose-binding protein (MBP) chaperone (366 amino acids) (*44*), a Gly-Gly-Gly-Gly tetrapeptide linker, a 5HVZ dimerization domain (49 amino acids), a Gly-Ser-Gly-Ser-Gly-Gly peptide linker, a TcdB-binding VHH (111-127 amino acids), a Gly-Ser-Gly tripeptide linker and a hexahistidine tag (543-562 amino acids total) (fig. S5A). The 5HVZ dimerization domain was derived from the mammalian cAMP-dependent protein kinase A (PKA) holoenzyme (*30*, *45*). Full-length PlyCD (pp1093) its catalytic domain alone, PlyCD1-174 (pp1092), were expressed in spirulina strains SP1286 and SP1287, respectively, with an N-terminal 6x his-tag.

Genes encoding pp1005, pp1006, pp1007, pp1093 and pp1092 were engineered into the spirulina chromosome by homologous recombination (fig. S5B) (*29*). The final strains contained the gene of interest integrated into the spirulina chromosome at a single, pre-selected location and no other exogenous genetic information. Clonal spirulina filaments were then isolated by micromanipulation, verified as being homozygous with respect to the transgene, and used to create a frozen strain bank (fig. S5, B and C) (*29*).

Characterization of spirulina-expressed anti-TcdB VHHs and anti-*C. difficile* lysin

Expression levels of all 5 candidate therapeutic proteins in spirulina were quantified using a capillary electrophoresis-based immunoassay (fig. S6A). The dimeric state of the VHHs on the 5HVZ scaffold was confirmed by comparing their relative mobilities during size-exclusion chromatography, and by capillary electrophoresis in reducing versus non-reducing conditions (fig. S6B). Intra-scaffold disulfide bonds were present in the extracted proteins (fig. 6SB) but were dispensable for stable assembly of the 5HVZ-VHH dimers (fig. S6C).

Following extraction from SP1286 and SP1287 biomass the pp1093 and pp1092 proteins were found to be monomeric by size-exclusion chromatography and non-reducing PAGE (fig. S7B). However, pp1093 exhibited notable size heterogeneity, with lower molecular size species. After aqueous extraction greater than 75% of pp1092 was soluble (fig. S7A).

The lytic activities of pp1093 and pp1092 extracted from SP1286 and SP1287 were compared in a turbidity reduction assay using *B. subtilis* as the target bacterium. The specific activity of pp1092 was 8-fold greater than pp1093 (fig. S7C). SP1287 was selected for inclusion in LMN-201 based upon its superior expression level, homogeneity and bioactivity compared to SP1286. As a control for interference, it was shown that pp1092 did not affect toxin neutralization by the anti-TcdB VHH cocktail (Fig. 2A).

Stabilities of spirulina-expressed anti-TcdB VHHs and anti-*C. difficile* lysin

The four therapeutic proteins within LMN-201 were tested for their resistance to intestinal proteases: trypsin, elastase, and chymotrypsin (fig. S8 and S9). When exposed to conditions simulating constitutive levels of these proteases for one hour, pp1005, pp1006, and pp1007 retained nearly 100% ELISA binding activity compared to undigested protein. At a higher concentration of protease that simulated the induced protease amounts following a meal, pp1005 and pp1006 exhibited some sensitivity to digestion with 0.1 mg/mL trypsin but still retained 63% and 75% of their antigen-binding activities, respectively (fig. S8A). To confirm that digestion did not affect bioactivity, chymotrypsin-digested pp1005, pp1006, and p1007 were also evaluated in a cell viability assay. No significant changes in toxin neutralizing activity were observed after exposure to chymotrypsin for at least one hour (fig. S8B).

Protease treated pp1092 was analyzed for structural integrity by SDS-PAGE (fig. S9, A and B), and for bioactivity in a turbidity reduction assay using intact *B. subtilis* as the substrate (fig. S9C). pp1092 showed no detectable change in molecular size (25kDa) following digestion with any of the three proteases. In contrast, full length PlyCD (37 kDa) was almost 100% cleaved to a smaller 25 kDa product by all three proteases, consistent with release of the smaller, protease-stable catalytic subdomain. Further, pp1092 retained 100% bioactivity following digestion with any of the three proteases at the lower level, and greater than 70% bioactivity following digestion with higher (induced) protease amounts.

Differences between competitive and independent binding of multiple antibodies

It is critical to establish whether simultaneous binding of antibodies can occur, or if antibody binding is exclusive. This addresses the critical question: can the target, *T*, bound by one antibody, *A*, be bound by another antibody, *B*, to form a trinary complex, *ABT*? If so, the binding is independent and the right column in Table 1 applies. If not, the binding is exclusive and the left column in Table 1 applies.

The difference between these two binding cases rests, fundamentally, in the difference between taking the sum of effects (competitive) or the product of effects (independent), providing a geometric advantage to the independent case. As an illustration, consider the case where $A/K_A=B/K_B=100$. In the competitive case, $\alpha=1+100+100=201$. In the independent case, $\alpha=1+100+100+100*100=10{,}201$. With three binders, $\alpha=1+(100)\cdot 3=301$ in the competitive case and $\alpha=(1+100)^3=1{,}030{,}301$ in the independent case. The competitive case increases α linearly with N binders, while the independent case increases α geometrically with N binders.

Returning to the TcdB case in affected patients, an $\alpha=150{,}000$-fold shift in TcdB potency can be achieved with three independent binders when $\alpha=150{,}000=(1+A/K_A)\cdot(1+B/K_B)\cdot(1+C/K_C)$, per Table 1. The minimum sum ratio of concentration to potency for each binder is $A/K_A = B/K_B = C/K_C = 52.1$-fold.

In contrast, an $\alpha=150{,}000$-fold shift in TcdB potency can be achieved with three competitive binders when $\alpha=150{,}000=1+A/K_A+B/K_B+C/K_C$, per Table 1. The minimum sum ratio of concentration to potency for each binder is $A/K_A = B/K_B = C/K_C = 50{,}000$-fold.

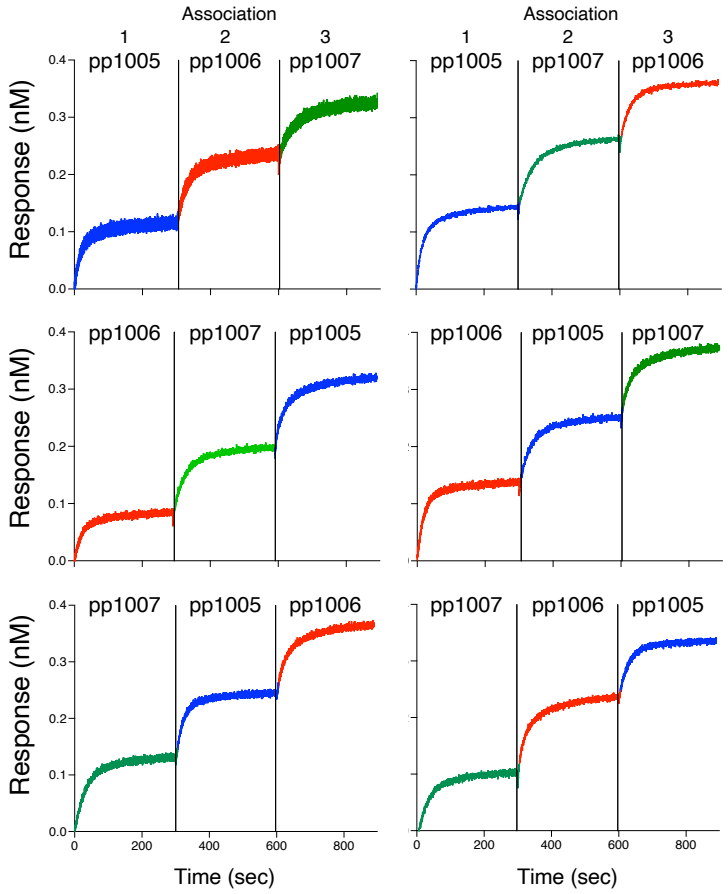

Fig. S1.

Tandem binding analysis of dimeric anti-TcdB VHHs. The binding responses were measured on an Octet Rad96e BLI instrument using EZ-link biotinylated inactive TcdB, immobilized on a streptavidin biosensor. Antigen-loaded biosensors were incubated with the first dimeric VHH (pp1005, pp1006, or pp1007) for 4 minutes in wells containing saturating VHH (2 µg/mL) to measure the first binding response. Biosensors were then moved to wells containing saturating amount of second dimeric VHH (pp1005, pp1006, or pp1007, at 2 µg/mL) and incubated for 4 minutes to assess second VHH binding to TcdB in the presence of the first VHH. To measure the tandem binding of all three VHHs, VHH1 and VHH2 bound TcdB containing biosensors were incubated in wells with saturating dimeric VHH3 (pp1005, pp1006, or pp1007, at 2 µg/mL). Binding is indicated by the increase in response where pp1006 binding is depicted with red, increase in signal due to pp1007 binding indicated with green seismograms and blue sonograms correspond to pp1005 binding.

A

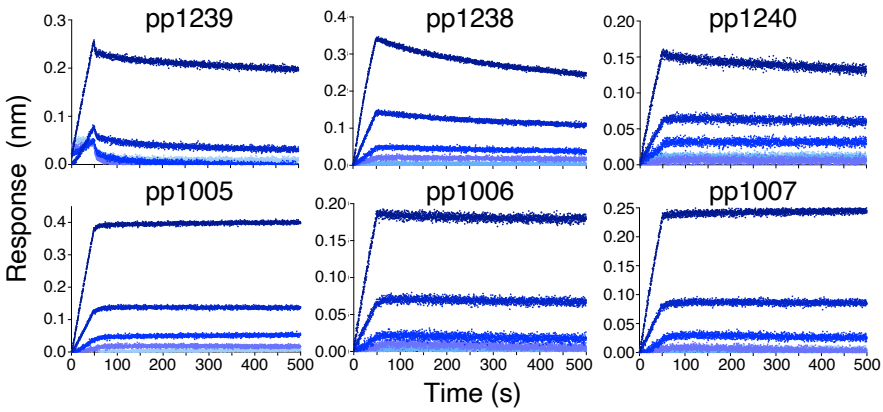

B

Sample ID	KD (nM)	k_a (1/Ms)	k_d (1/s)
pp1239 (M)	2.56 (0.02)	1.64E+05 (0.12)	4.20E-04 (0.13)
pp1005 (D)	0.002 (0)	1.16E+05 (0.11)	2.59E-07 (0)
pp1238 (M)	4.85 (0.06)	1.45E+05 (0.02)	7.02E-04 (0.02)
pp1006 (D)	0.03 (0)	7.48E+04 (1.68)	2.57E-06 (0)
pp1240 (M)	2.09 (0.06)	1.26E+05 (0.04)	2.63E-04 (0.03)
pp1007 (D)	0.58 (0.07)	1.54E+05 (0.17)	8.97E-05 (0.30)

Fig. S2.

Binding affinities of TcdB VHHs. (**A**) BLI binding sensorgrams analysis of binding kinetic for anti-TcdB VHHs as monomers (pp1239, pp1238, and pp1240) and dimers (pp1005, pp1006, and pp1007). (**B**) The rate constants k_a and k_d were calculated from concentration-dependent responses. The apparent equilibrium binding constant (K_D) for each was determined from the rate of association (k_a), and rate of dissociation (k_d). Values of K_D, k_a and k_d are indicated in the table (M, monomer; D, dimer).

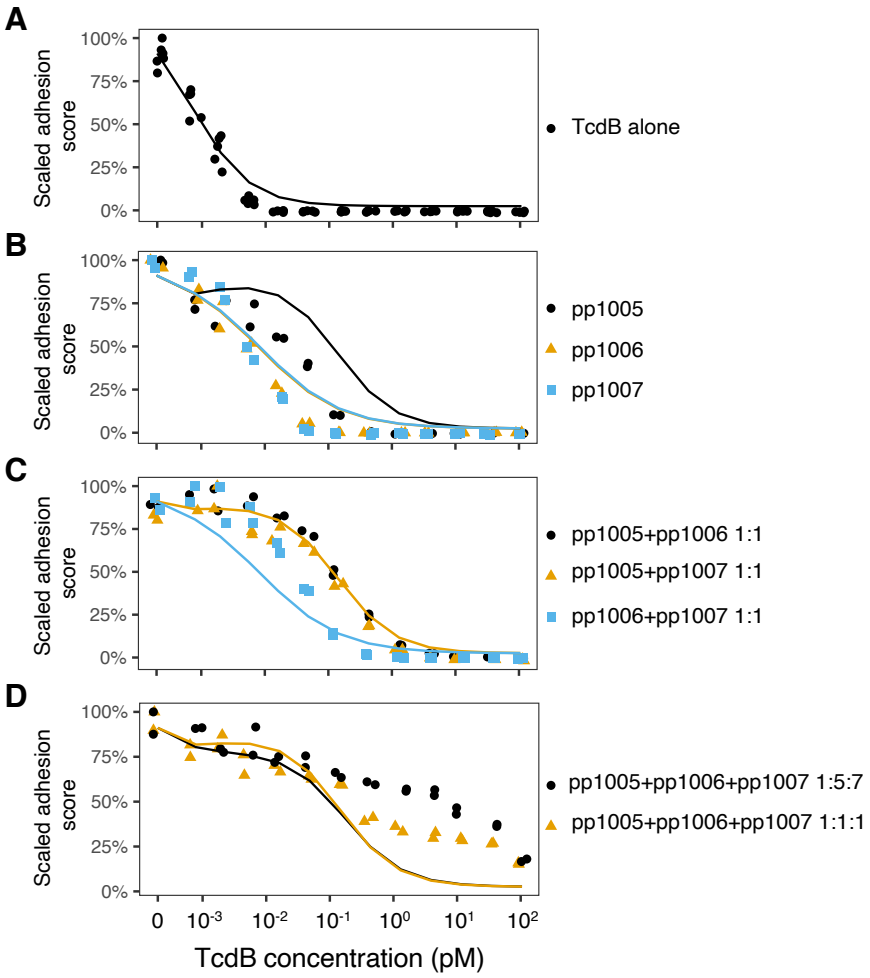

Fig. S3.

Alternative model – Competitive Binding. Illustrated is the (alternative) competitive model fit, where it is assumes that the VHHs do not act independently. The independent model (BIC=-714) was strongly preferred over the competitive model (BIC=-273). The model fit to the TcdB-only (**A**) data shows overprediction around 0.003 pM, effectively underestimating the potency of TcdB to allow better capture of the overall data set. Singleton pp1005 (**B**) is overpredicted, duel pp1006+pp1007 (**C**) is underpredicted, and both triple cocktails (**D**) are strongly underpredicted. Essentially, the competitive model cannot adjudicate the extremely potent triple cocktails and lower potency singleton and dual agents with the additive assumption.

A comparison to the final independent model (Equation S1) can be made for the competitive model alternative:

$$\alpha = 1 + \sum_{i=1}^{N} \frac{I_i}{K_i} = 1 + \frac{E_{max}^{pp1005} \cdot \left(A^{pp1005}\right)^H}{\left(A^{pp1005}\right)^H + \left(EC_{50}^{pp1005}\right)^H} + \frac{A^{\boldsymbol{pp1006}}}{EC_{50}^{\boldsymbol{pp1006}}} + \frac{A^{\boldsymbol{pp1007}}}{EC_{50}^{\boldsymbol{pp1007}}} \quad \text{(S1)}$$

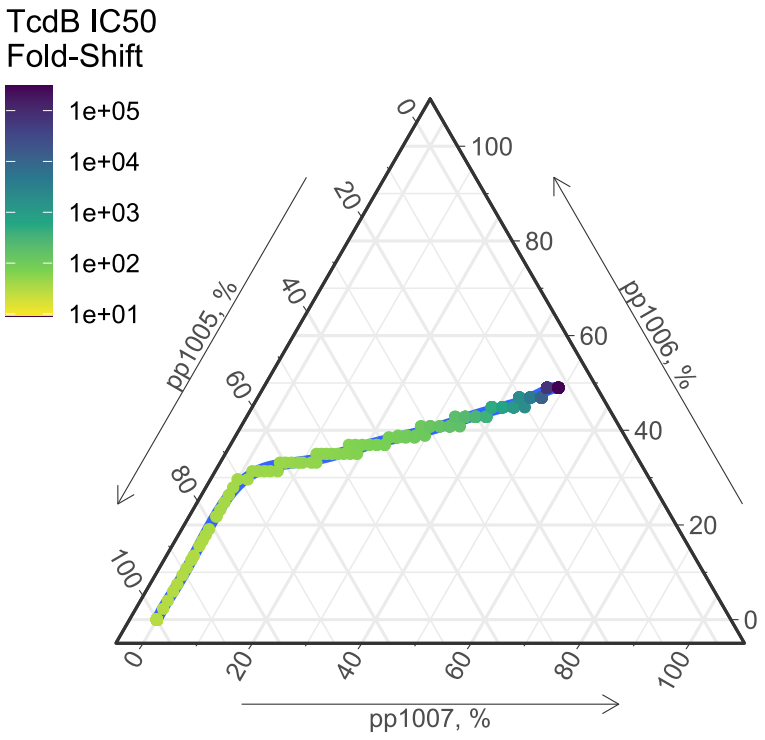

Fig. S4.

Optimizing the Synthetic Antagonism of a Cocktail. Ternary plot showing the optimal mixture of pp1005: pp1006: pp1007 across a total VHH concentration of 0.01 to 10 nM. At 0.01 nM total VHH, 100% pp1005 (lower left corner) is optimal due to its high potency relative to pp1006 and pp1007 which matches the result in Fig. 3A. As the ratio of VHH concentrations to their potency exceeds 1.0, the geometric advantage of synthetic antagonism results in a mixture of VHHs (centroid of the diagram) which matches the result in Figure 3, Panels B and C. As the effect of pp1005 saturates, its presence in the mixture decreases, leading to a path approaching a binary mixture of pp1006 and pp1007 which matches the results in Figure 3, Panel D. Additional simulations across a range of total VHH concentration from 0.01 nM to 10 nM were performed to understand the change in optimal cocktail fractions. Similar to Figure 3 in the main text that describes four levels of total VHH, α in Equation 1S was maximized by nonlinear optimization subject to the mixture constraint (sum to 1.0) and total VHH concentration. Supplemental Figure 4 shows the optimal mixture as a path with increasing total VHH concentration. Additionally, the ternary diagram is annotated with the fold-shift if the 10 nM of total VHH were instead apportioned to 100% pp1005 (45-fold, left corner), pp1006 (180-fold, upper corner) or pp1007 (140-fold, right corner). Fold shift for 1:1 mixtures are shown on their respective edges, the 1:1:1 mixture is shown at the centroid (140,000 fold), and the 1:5:7 mixture is shown in blue (260,000-fold) near the 1:1 mixture of pp1006:pp1007.

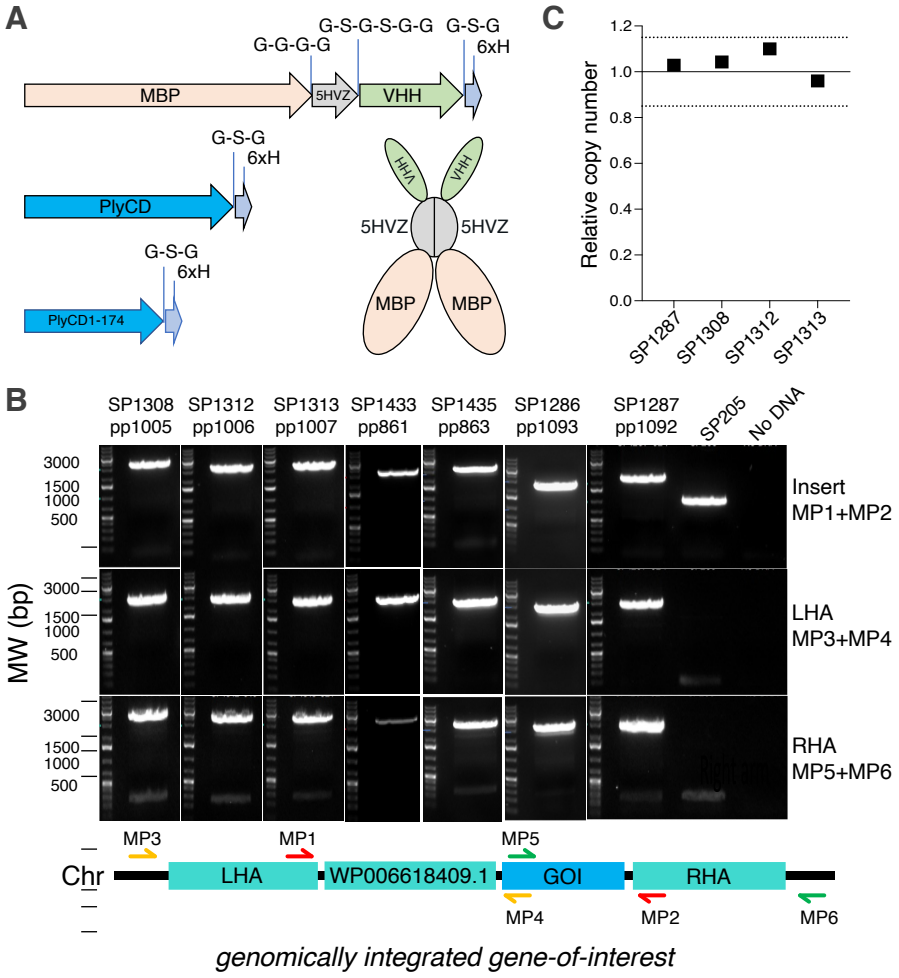

Fig. S5.

Spirulina strain engineering and characterization. (**A**) Diagram of modified anti-*C. difficile* TdcB VHHs 5D, E3, 7F, PlyCD, PlyCD$_{1\text{-}174}$, and 5HVZ-mediated dimer formation. (**B**) A schematic diagram of the genomic integration locus (WP_006618409.1). PCR was performed with indicated primers to analyze the segregation and specificity of integration for each strain. PCR products with primers MP1/MP2 showed bands of predicted sizes in all strains, and absence of the parental alleles, suggesting the segregation to homozygosity was complete. The primer pairs for amplification of the left homology arm (LHA) and right homology arm (RHA) include one priming site (MP3 and MP6) that is only present in the spirulina genome at the target locus and absent from the donor plasmid. PCR amplification of the LHA and RHA with MP3/MP4 and MP5/MP6, respectively, demonstrated that genomic integration was site-specific. The DNA sequences from all PCR products were verified to match expectations. (**C**) Copy numbers of the genes of interest (GOIs) were determined with next-generation sequencing by comparing reads of the GOIs to ten randomly selected native spirulina genes. Dotted line indicates range in which the relative copy numbers were considered equivalent to one.

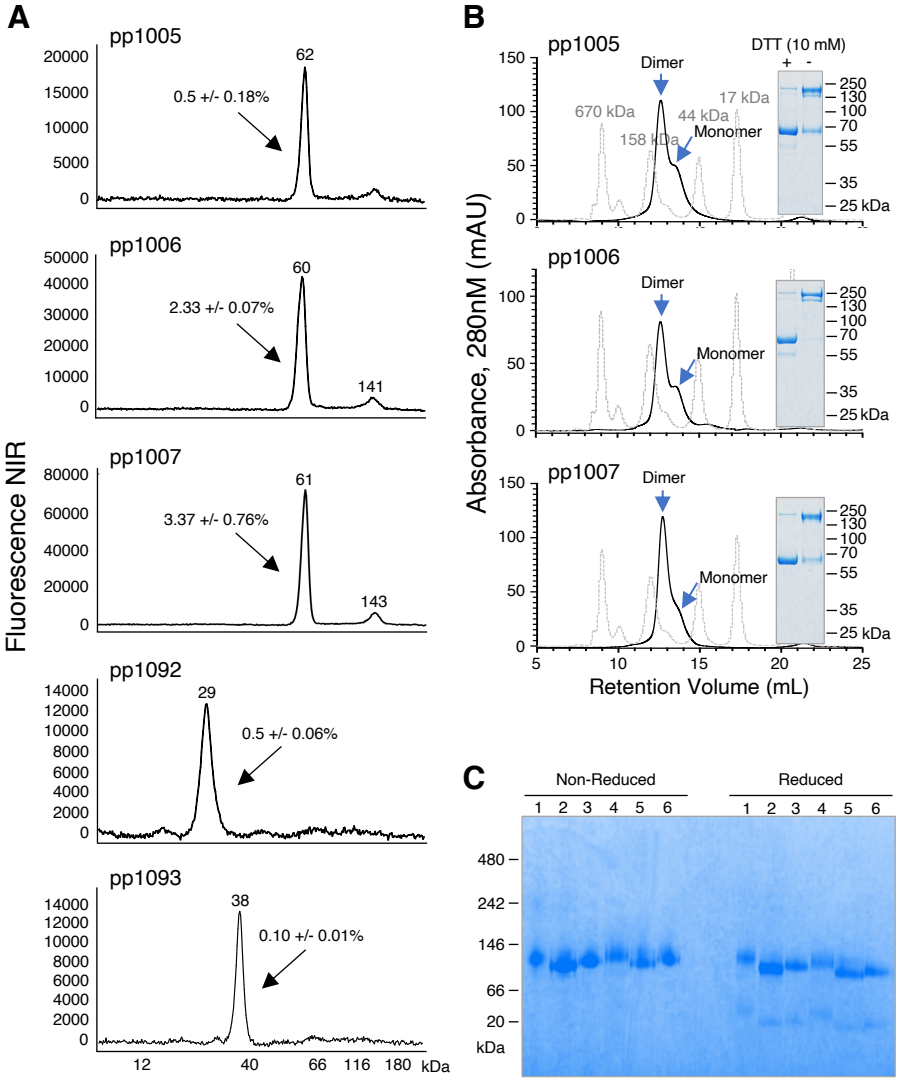

Fig. S6.

Characterization of spirulina-expressed anti-TcdB VHHs and lysins. (**A**) Chromatograms of pp1005, pp1006, pp1007, pp1092, and pp1093 extracted from spirulina biomass and detected under reducing conditions using a capillary electrophoresis-based immunoassay. Soluble protein, as a percentage of dry weight, is indicated on each graph. (**B**) Spirulina expressed and purified pp1005, pp1006, and pp1007 in aqueous solution (PBS, pH 7.4) assayed on a Superdex 200 10/300 GL FPLC column. Grey peaks correspond to molecular size standards. The monomeric and dimeric portions of the VHHs are indicated. Disulfide bond formation between monomers was assessed using denaturing gel electrophoresis under non-reducing and reducing (50 mM DTT) conditions. (**C**) Native gel electrophoresis analysis of pp1005

1 (1, 4), pp1006 (2, 5), and pp1007 (3, 6) under non-reducing or reducing (50 mM DTT) conditions. In the
2 presence of reducing agent the dimeric state of the VHHs was mostly preserved.

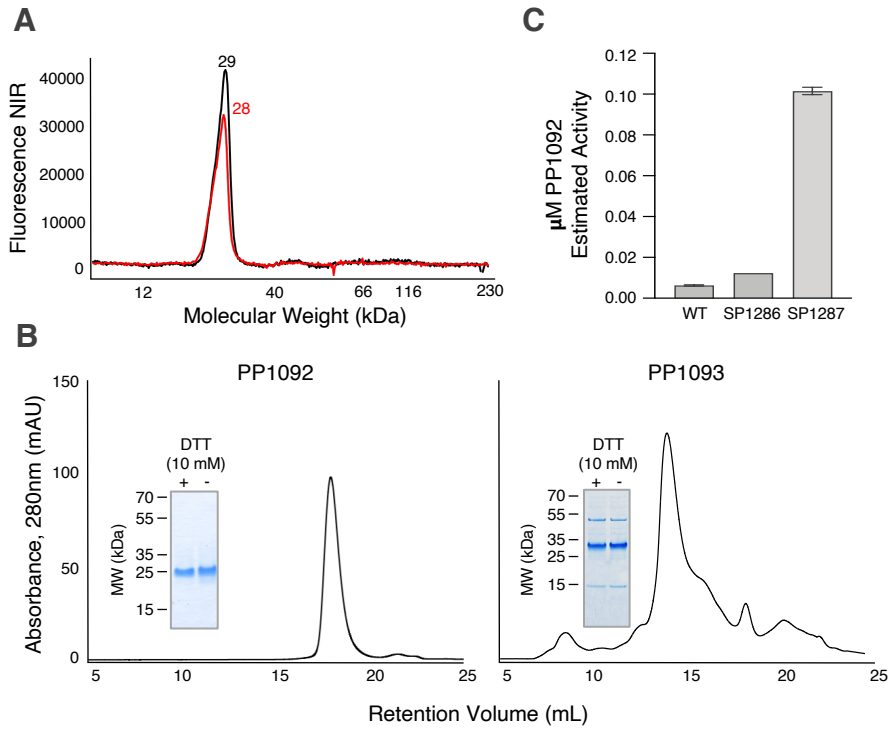

Fig. S7.

Characterization of spirulina-expressed anti-*C. difficile* lysin. (**A**) A chromatogram of pp1092 after total protein extraction (black) and soluble protein extraction (red). More than 75% of the lysin protein is soluble. (**B**) Spirulina-expressed, purified lysins, pp1092 and pp1093, in aqueous solution (1xPBS, pH 7.4) evaluated by size-exclusion chromatography (Superdex 200 10/300 GL FPLC column). Purified protein samples were also assessed using denaturing gel electrophoresis under non-reducing and reducing (50 mM DTT) conditions. (**C**) Activity of spirulina extracts (wild-type (WT) expressing no lysin, SP1286 expressing pp1093, and SP1287 expressing pp1092) prepared at 2 mg/mL were compared by measuring the time to reduce turbidity of living *B. subtilis* SL4 cultures by 50%.

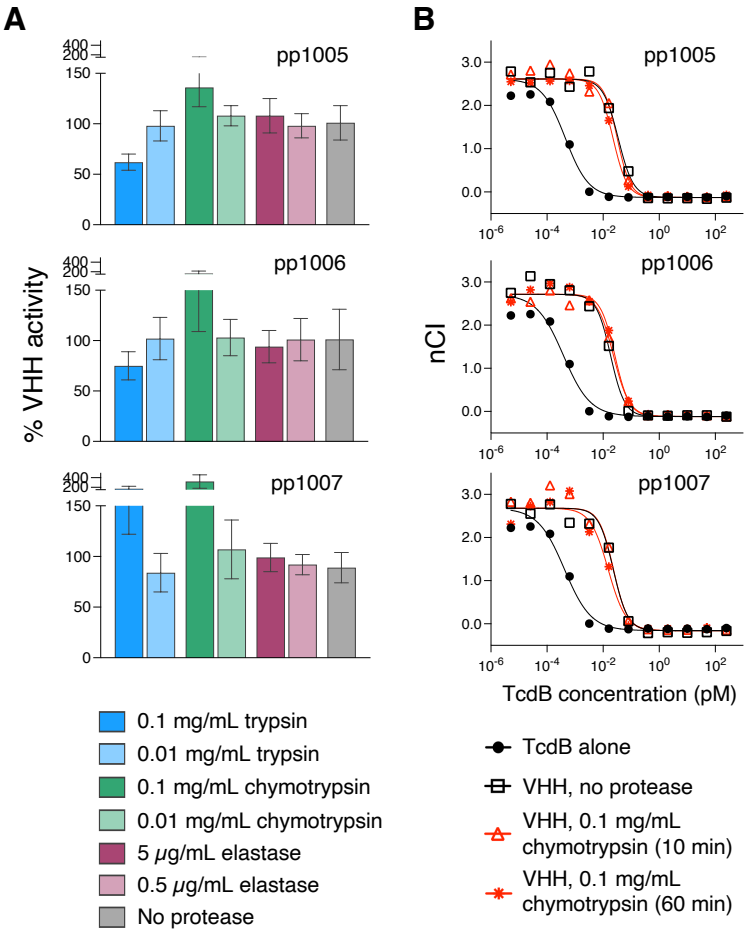

Fig. S8.

Stability of anti-TcdB VHHs to gastrointestinal proteases. (**A**) The percentage of TcdB-binding activity of pp1005, pp1006, and pp1007 measured by ELISA after digestion with trypsin, chymotrypsin, and elastase. Two concentrations of each protease were tested to simulate either "fed" (higher concentration) or "fasted" (lower concentration) conditions. Data represent the average of six independent replicates, the error bars representing the standard deviation. (**B**) TcdB-neutralizing activity of protease digested pp1005, pp1006, and pp1007. VHH homodimers treated with chymotrypsin for either 10 or 60 minutes were compared with the corresponding undigested protein. Each was diluted to a fixed concentration (pp1005 was 0.05 nM, pp1006 was 5 nM, and pp1007 was 5 nM) and incubated with serially diluted TcdB-10463. Each mixture was assayed for its effect on cell adhesion. After digestion all exhibited neutralizing activities similar to undigested controls.

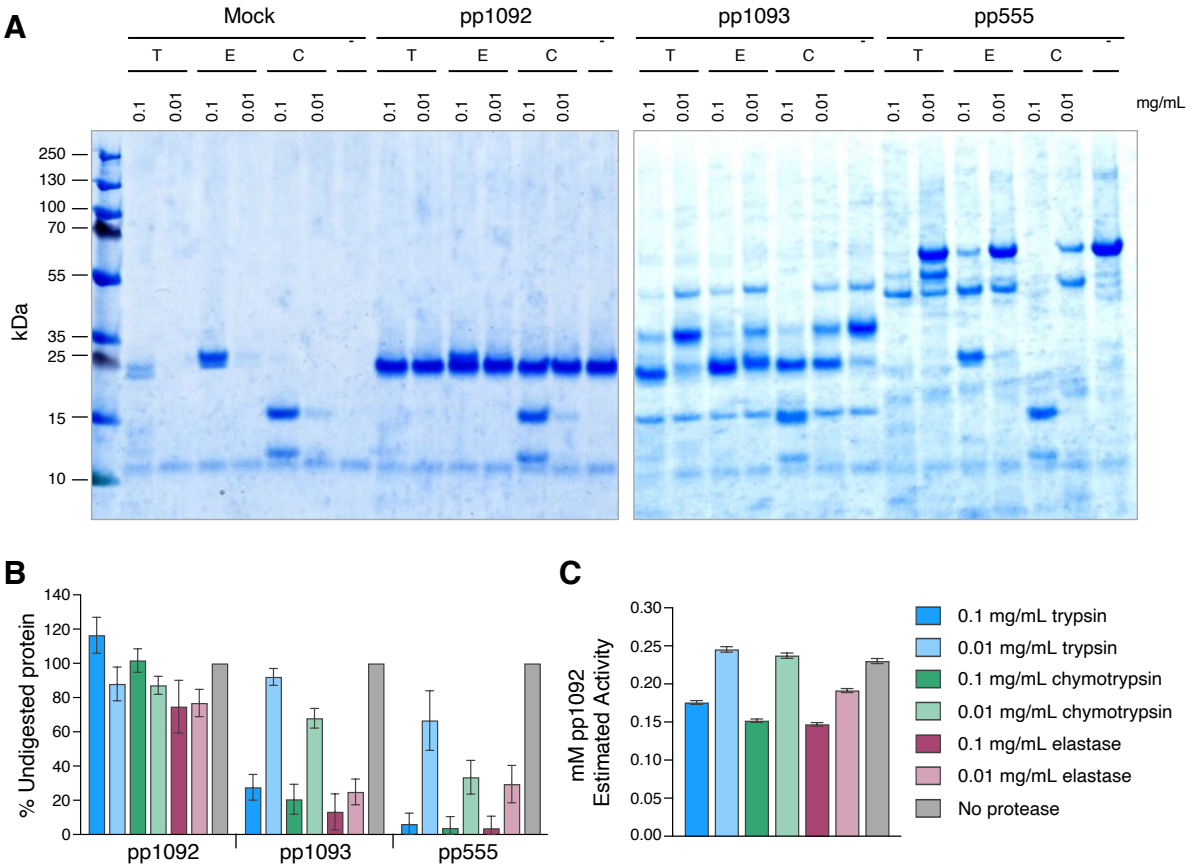

Fig. S9.

Stability of anti-*C. difficile* lysin to gastrointestinal proteases. (**A**) Full-length lysin (pp1093, 37 kDa), its catalytic subdomain (pp1092, 25 kDa), and a protease sensitive VHH (pp555, 55 kDa) were digested with trypsin (T), chymotrypsin (C), and elastase (E) at pH 6.4 for 1 hour at 37 °C, quenched with protease inhibitors, the products separated by size using PAGE, and peptides visualized by Coomassie staining. Mock digestions without target proteins were performed to visualize the contribution by the proteases and quenching reagents. (**B**) The image in A (representative of six independent digestions) was quantified by densitometry with error expressed as SEM. (**C**) Activities of pp1092 digests were measured by determining the time to reduce the turbidity of a culture of live *B. subtilis* SL4 by 50%. This value was then plotted against a standard curve of undigested reference lysin to determine the activities of the digested samples compared to undigested reference lysin. Error bars represent the standard error calculated from three technical replicates.

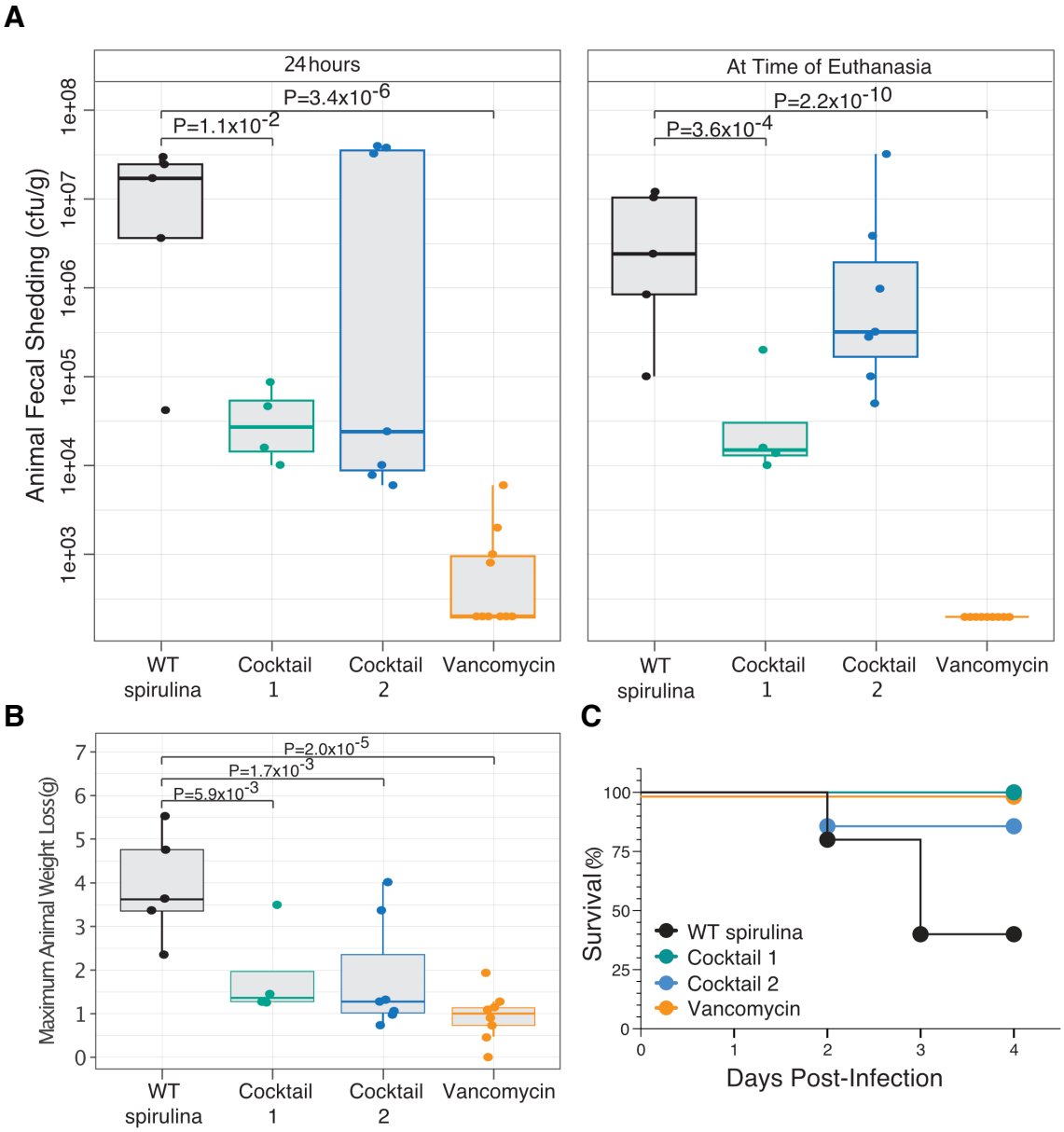

Fig. S10.

Mouse challenge study. Shown are (**A**) fecal spore counts 24 hours after infection and at the time of euthanasia; (**B**) maximum weight loss for individuals in each group; and (**C**) Kaplan-Meier representation of survival. Individuals were euthanized upon losing ≥15% of their initial weight. Individuals in panels A and B are represented as a point and the group median, interquartile range (IQR) and 1.5*IQR as boxplots. A) Log_{10} fecal shedding data were fit with a linear model with group as a predictor per time point. Treatment group is a significant predictor ($p<0.05$) of shedding relative to the wild-type spirulina group (control/intercept) for Cocktail 1 and vancomycin. Cocktail 2 fails significance testing ($p\sim0.1$ and $p\sim0.25$). Statistic reports the t ratio based on a Student t reference distribution, and p-value reports the two-tailed p-value corresponding to the t ratio based on the Student t reference distribution. B) Maximum animal

weight loss was fit with a linear model with treatment as predictors of weight loss. Treatment group is a significant predictor ($p<0.05$) of animal weight loss relative to the wild-type spirulina group (control). C) Kaplan-Meier survival curves for mice infected with 10^5 *C. difficile* spores and treated with vancomycin (orange, n=10), wild-type spirulina (black, n=5), spirulina therapeutic Cocktail 1 (teal, n=5) or Cocktail 2 (blue, n=7). Survival rates were compared to treatment with wild-type spirulina by log-rank test. Significance was observed with vancomycin treatment ($p=0.0068$), borderline significance was observed with spirulina Cocktail 1 ($p=0.080$) and Cocktail 2 ($p=0.14$) treatment.

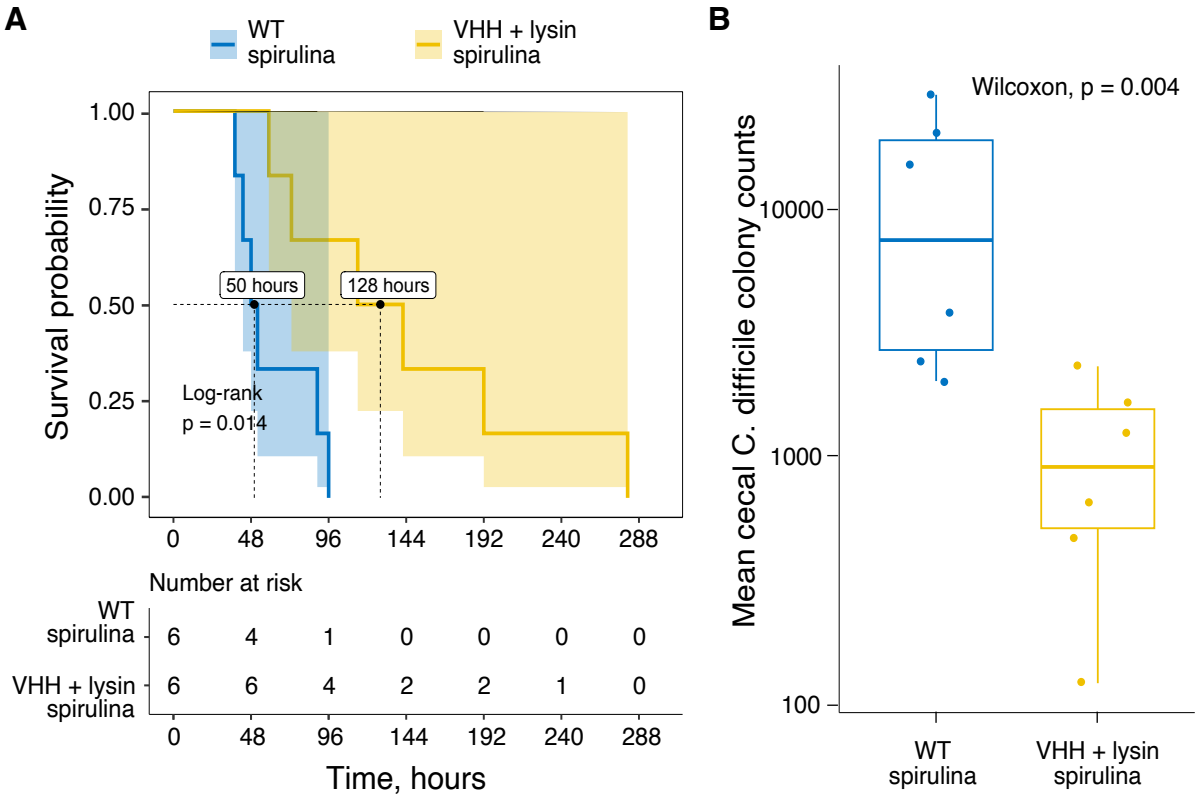

Fig. S11.

Hamster challenge trial. (**A**) The Lumen therapeutic (VHH+lysin spirulina) prolonged survival times when compared to the negative control wild-type spirulina (WT spirulina). Clindamycin-treated Golden Syrian hamsters were administered phosphate-buffered saline, wild-type spirulina, or the Lumen therapeutic two times a day starting one day before infection with *C. difficile* (15,000 spores) and continuing until they reached their humane endpoints or the end of the study (14 days post-infection). The median survival times for each group were compared log-rank test. (**B**) The Lumen therapeutic decreased *C. difficile* cecal colonization when compared to the negative control wild-type spirulina. Cecal contents were collected after animals reached their humane endpoints or the termination date. *C. difficile* colony counts were quantified by comparing RT-PCR measurements of extracted DNA from these samples as compared to a standard curve generated by DNA extracted from vegetative *C. difficile* cells. Fewer *C. difficile* cells colonized the cecum in hamsters treated with the Lumen therapeutic than in wild-type spirulina-treated or untreated groups. Colony counts were compared by Wilcoxon rank sum test (Mann-Whiney test) with continuity correction.

Table S1.

Final Independent parameters. During analysis of the data, it became apparent than the linear concentration-potency relationship, $1+C_{pp1005}/K_{pp1005}$, was incompatible with the observed data for pp1005. Specifically, the independent model for three binders (from Table 1) would be:

$$\alpha = \prod_{i=1}^{N}\left(1+\frac{I_i}{K_i}\right) = \left(1+\frac{A^{pp1005}}{EC_{50}^{pp1005}}\right)\cdot\left(1+\frac{A^{pp1006}}{EC_{50}^{pp1006}}\right)\cdot\left(1+\frac{A^{pp1007}}{EC_{50}^{pp1007}}\right) \quad (2S)$$

The linear concentration-potency relationship expresses a surmountable inhibition of TcdB, meaning that any concentration of TcdB can be overcome by enough VHH. This was the case for pp1006 and pp1007, but pp1005 exhibited a limit to the fold-shift possible inhibition in a concentration-dependent manner suggesting insurmountable inhibition of TcdB. As such, the concentration-potency model for pp1005 was altered to be saturable, specifically using a Michaelis-Menten model with Hill slope coefficient. Expanding the preferred independent binding model for all three VHHs:

$$\alpha = \left(1+\frac{E_{max}^{pp1005}\cdot\left(A^{pp1005}\right)^{H}}{\left(A^{pp1005}\right)^{H}+\left(EC_{50}^{pp1005}\right)^{H}}\right)\cdot\left(1+\frac{A^{pp1006}}{EC_{50}^{pp1006}}\right)\cdot\left(1+\frac{A^{pp1007}}{EC_{50}^{pp1007}}\right) \quad (3S)$$

EC_{50} values for the VHHs were determined from the totality of the data, which included not only single VHHs but also all double and triple combinations. The VHH concentration (EC_{50}) needed to cause a two-fold increase in TcdB IC_{50} for pp1005, pp1006 and pp1007 was 21.44, 54.13, and 69.26 pM, respectively; pp1005 exhibited saturable inhibition with a maximal fold-increase of TcdB IC_{50} by 45.25-fold (E_{max}^{pp1005}) with a Hill slope coefficient of 1.813 (H).

Term	Estimate	Standard Error	p-value	2.5 CI %	97.5 CI %
IC_{50}^{TcdB}, pM	0.001268	6.573e-05	2.238e-52	0.001138	0.001397
H^{TcdB}, (unitless)	1.495	0.07091	1.352e-58	1.355	1.634
EC_{50}^{pp1005}, nM	0.02144	0.002423	1.277e-16	0.01667	0.02622
H^{pp1005}, (unitless)	1.813	0.1245	1.121e-35	1.567	2.058
E_{max}^{pp1005}, fold	45.25	3.076	3.204e-36	39.2	51.31
EC_{50}^{pp1006}, nM	0.05413	0.003761	4.25e-35	0.04673	0.06154
EC_{50}^{pp1007}, nM	0.06926	0.004852	1.107e-34	0.05971	0.07882

Table S2.

Full model for fecal shedding at 24 hours and at euthanasia. Log_{10} fecal shedding data were fit with a linear model with group as a predictor per time point. Model estimates are also provided in the table. Treatment group is a significant predictor ($p<0.05$) of shedding relative to the wild-type spirulina group (control/intercept) for Cocktail 1 and vancomycin. Cocktail 2 fails significance testing ($p\sim0.1$ and $p\sim0.25$). Statistic reports the t ratio based on a Student t reference distribution, and p-value reports the two-tailed p-value corresponding to the t ratio based on the Student t reference distribution. For the wild-type spirulina group, the estimate reports the mean of the log CFU/g values; for the other treatment arm, the estimate reports the difference in log CFU/g values relative to the wild-type spirulina group and the associated t-test against this reference group results.

Collection Time	Term	Estimate	Std. error	Statistic	p value
24 hours	**Wild-type spirulina**	6.656	0.5276	12.62	1.51E-11
	Vs. Cocktail 1	-2.206	0.7914	-2.787	1.08E-02
	Vs. Cocktail 2	-1.123	0.6908	-1.626	1.18E-01
	Vs. Vancomycin	-3.977	0.6462	-6.155	3.40E-06
Euthanasia	**Wild-type spirulina**	6.28	0.296	21.22	3.85E-16
	Vs. Cocktail 1	-1.867	0.4439	-4.206	3.65E-04
	Vs. Cocktail 2	-0.4623	0.3875	-1.193	2.46E-01
	Vs. Vancomycin	-3.979	0.3625	-10.98	2.16E-10

Table S3.

Full model for maximum animal weight loss. Maximum animal weight loss was fit with a linear model with treatment as predictor of weight loss. Model estimates are given in grams, with wild-type spirulina as the reference and the other treatment estimates as deltas from that estimate. Treatment group is a significant predictor ($p<0.05$) of animal weight loss relative to the wild-type spirulina group (control).

Term	Estimate	Std. error	Statistic	p value
Wild-type spirulina	3.922	0.4504	8.708	1.405E-08
Vs Cocktail 1	-2.057	0.6756	-3.045	5.95E-03
Vs Cocktail 2	-2.102	0.5897	-3.564	1.73E-03
Vs Vancomycin	-2.984	0.5516	-5.409	1.97E-05